Article

SOURCE DATA | TRANSPARENT PROCESS | OPEN ACCESS

THE EMBO JOURNAL

Functional genomics identifies a requirement of pre-mRNA splicing factors for sister chromatid cohesion

Sriramkumar Sundaramoorthy[1,†], María Dolores Vázquez-Novelle[1], Sergey Lekomtsev[1,‡], Michael Howell[2] & Mark Petronczki[1,*]

Abstract

Sister chromatid cohesion mediated by the cohesin complex is essential for chromosome segregation during cell division. Using functional genomic screening, we identify a set of 26 pre-mRNA splicing factors that are required for sister chromatid cohesion in human cells. Loss of spliceosome subunits increases the dissociation rate of cohesin from chromatin and abrogates cohesion after DNA replication, ultimately causing mitotic catastrophe. Depletion of splicing factors causes defective processing of the pre-mRNA encoding sororin, a factor required for the stable association of cohesin with chromatin, and an associated reduction of sororin protein level. Expression of an intronless version of sororin and depletion of the cohesin release protein WAPL suppress the cohesion defect in cells lacking splicing factors. We propose that spliceosome components contribute to sister chromatid cohesion and mitotic chromosome segregation through splicing of sororin pre-mRNA. Our results highlight the loss of cohesion as an early cellular consequence of compromised splicing. This may have clinical implications because *SF3B1*, a splicing factor that we identify to be essential for cohesion, is recurrently mutated in chronic lymphocytic leukaemia.

Keywords chromosome; cohesin; cohesion; mitosis; splicing
Subject Categories DNA Replication, Repair & Recombination; RNA Biology
DOI 10.15252/embj.201488244 | Received 14 February 2014 | Revised 3 August 2014 | Accepted 18 August 2014 | Published online 25 September 2014
The EMBO Journal (2014) 33: 2623–2642

See also: **J Valcárcel & M Malumbres** (November 2014) and **P van der Lelij *et al*** (November 2014)

Introduction

The correct partitioning of sister genomes during cell division requires that sister kinetochores attach to microtubules emanating from opposite spindle poles. To facilitate this, sister chromatids are held together from their synthesis during DNA replication until their disjunction by a phenomenon called sister chromatid cohesion (Guacci *et al*, 1994; Nasmyth & Haering, 2009). Sister chromatid cohesion is mediated by a ring-shaped tripartite protein complex called cohesin that is composed of the core subunits SMC3, SMC1 and SCC1 and that is thought to topologically entrap sister chromatids (Haering *et al*, 2008).

A number of accessory factors regulate the function and properties of cohesin throughout the cell cycle. Cohesin loading onto chromatin happens during telophase/G1 and is performed by a cohesin-loading complex composed of SCC2 and SCC4 proteins (Ciosk *et al*, 2000). At this stage, cohesin interacts with chromatin transiently (Gerlich *et al*, 2006). A stable cohesin–chromatin liaison is prevented by the activity of the WAPL–PDS5 protein complex (Tanaka *et al*, 2001; Gandhi *et al*, 2006; Kueng *et al*, 2006; Sutani *et al*, 2009). The cohesin release protein WAPL is thought to remove cohesin rings from chromatin by opening the SMC3–SCC1 interface of the complex (Chan *et al*, 2012; Buheitel & Stemmann, 2013; Eichinger *et al*, 2013). The subsequent establishment of sister chromatid cohesion requires DNA replication (Uhlmann & Nasmyth, 1998) as well as the opposition of WAPL–PDS5 activity by the acetylation of cohesin's SMC3 subunit at the hands of the acetyltransferases ESCO1/2 (Rolef Ben-Shahar *et al*, 2008; Unal *et al*, 2008; Zhang *et al*, 2008; Rowland *et al*, 2009; Chan *et al*, 2012). In vertebrate cells, sister chromatid cohesion and the stable association of cohesin with chromatin after DNA replication also require a protein called sororin (Rankin *et al*, 2005; Schmitz *et al*, 2007). DNA replication and SMC3 acetylation promote the binding of sororin to PDS5 leading to the displacement of WAPL (Lafont *et al*, 2010; Nishiyama *et al*, 2010). By antagonizing the cohesin release activity of WAPL, sororin is thought to ensure the long-lived links that hold sister chromatids together until mitosis (Gerlich *et al*, 2006; Schmitz *et al*, 2007; Lafont *et al*, 2010; Nishiyama *et al*, 2010).

In vertebrate cells, cohesin is removed in two discrete steps during mitosis (Waizenegger *et al*, 2000). The first step takes place during

1 Cell Division and Aneuploidy Laboratory, Cancer Research UK London Research Institute, Clare Hall Laboratories, South Mimms, Hertfordshire, UK
2 High-throughput Screening Laboratory, Cancer Research UK, London Research Institute, London, UK
*Corresponding author. Tel: +44 1707 625837; E-mail: mark.petronczki@cancer.org.uk
†Present address: Department of Pathology and Cell Biology, Columbia University Medical Center, New York, NY, USA
‡Present address: Medical Research Council Laboratory of Molecular Cell Biology, University College London, London, UK

prophase and requires WAPL as well as the phosphorylation of cohesin subunits and regulators by mitotic kinases (Losada *et al*, 2002; Sumara *et al*, 2002; Gimenez-Abian *et al*, 2004; Hauf *et al*, 2005; Kueng *et al*, 2006; Nishiyama *et al*, 2013; Tedeschi *et al*, 2013). This process, called the prophase pathway, removes cohesin from chromosome arms in a proteolysis-independent manner. Centromeric cohesin is rendered immune to the prophase pathway by the activity of the shugoshin protein Sgo1 (Kitajima *et al*, 2004; Salic *et al*, 2004; McGuinness *et al*, 2005). This maintains the connection between sister chromatids at the centromere and allows the correct attachment of chromosomes to the mitotic spindle. At anaphase onset, the remaining centromeric cohesin complexes are removed from chromatin through proteolytic cleavage of the SCC1 subunit leading to the segregation of sister chromatids towards opposite poles (Uhlmann *et al*, 2000; Hauf *et al*, 2001; Oliveira *et al*, 2010).

In addition to its function in chromosome segregation, cohesin plays important roles in other nuclear processes including the DNA damage response and DNA repair (Kim *et al*, 2002; Yazdi *et al*, 2002; Strom *et al*, 2004; Unal *et al*, 2004; Watrin & Peters, 2009), chromatin organization and gene regulation. Cohesin facilitates transcriptional termination between convergent genes in yeast (Gullerova & Proudfoot, 2008) and controls the developmentally regulated expression of genes in multiple systems (Rollins *et al*, 2004; Horsfield *et al*, 2007; Landeira *et al*, 2009; Pauli *et al*, 2010). Furthermore, cohesin acts in concert with the insulator protein CTCF (CCCTC binding factor) to promote long-range intra-chromatid interactions that govern gene expression (Parelho *et al*, 2008; Rubio *et al*, 2008; Stedman *et al*, 2008; Wendt *et al*, 2008; Hadjur *et al*, 2009; Sofueva *et al*, 2013; Zuin *et al*, 2014). Thus, cohesin has emerged as a key regulator of gene expression.

Conversely, increasing evidence suggests that gene expression processes impact on the function and properties of cohesin. In budding yeast, cohesin concentrates in regions of convergent transcription (Lengronne *et al*, 2004). SRm160, a protein belonging to the SR family of pre-mRNA splicing regulators, was found to associate with core cohesin subunits (McCracken *et al*, 2005). Also, depletion of UAP56 and URH49 helicases, members of the TREX complex that couple transcription and pre-mRNA processing with mRNA export (Lee & Tarn, 2013), led to alterations in cohesion in mitotic cells (Yamazaki *et al*, 2010).

In a search for novel factors controlling mitosis in human cells, we identify an essential and widespread role for pre-mRNA splicing factors in sister chromatid cohesion and provide a mechanistic explanation for their involvement during mitosis.

Results

A screen for potential new mitotic regulators identifies MFAP1

Genome-wide RNAi screens for cell cycle regulators (Mukherji *et al*, 2006; Kittler *et al*, 2007; Conery & Harlow, 2010; Neumann *et al*, 2010) and the proteomic analysis of the mammalian midbody (Skop *et al*, 2004) have highlighted candidate proteins that could represent novel factors involved in cell division. Using published data sets from these approaches, we compiled a list of 718 human candidate genes (Supplementary Fig S1A and Supplementary Table S1) for rescreening by RNA interference-mediated gene depletion in HeLa Kyoto cervical carcinoma cells. Established regulators of cell division and suspected pseudogenes were removed from the list (See Materials and Methods section for gene selection details). The screen utilized an arrayed siRNA library containing pools of four small interfering RNA (siRNA) duplexes for each of the 718 genes. We employed a fluorescence microscopy-based end point assay to detect nuclear defects in interphase cells that could be indicative for defects in cell division. In brief, HeLa Kyoto cells were transfected with siRNA pools in 96-well plates, grown for 52 h, fixed, labelled with a DNA dye and whole-cell stain, and subjected to automated image acquisition. Image data from three screen replicates were scored for the fraction of interphase cells displaying nuclear abnormalities, including multi-nucleation and nuclear fragmentation (Supplementary Fig S1B and Supplementary Table S1). siRNA pools targeting positive control genes, such as the essential cytokinesis regulator ECT2 (Yuce *et al*, 2005), scored with high phenotypic penetrance indicating effective target depletion in the screen (Supplementary Fig S1B and C).

Fifty candidate genes whose siRNA pools induced abnormal nuclear morphology in more than 20% of interphase cells were selected for further analysis. The selected genes were subjected to deconvolution analysis in which cells were transfected with the individual siRNA duplexes that constituted the pool of four duplexes used in the primary screen. For seven genes, two or more out of four siRNA duplexes recapitulated the phenotype observed in the primary screen (Supplementary Table S2). Transfection of the siRNA pool and of all four individual siRNA duplexes targeting the gene *MFAP1* (microfibrillar-associated protein 1) caused severe nuclear fragmentation characterized by the formation of small and large karyomeres and an increase in DNA content (Fig 1A and Supplementary Fig S1C). Consistent with an on-target effect, we found that the 4 siRNA duplexes also decreased MFAP1 protein levels (Fig 1A). MFAP1 siRNA #3 was selected for further analyses. MFAP1 is a conserved 52 kDa nuclear protein that has been purified in human spliceosomal fractions (Jurica & Moore, 2003). The *Drosophila* orthologue of MFAP1 associates with factors of the spliceosomal tri-small nuclear ribonucleoprotein (tri-snRNP) complex and has been implicated in pre-mRNA processing (Andersen & Tapon, 2008). The nuclear defects observed upon depletion of MFAP1 in human cells (Fig 1A) raise the possibility that this splicing factor is required for the segregation of chromosomes during cell division.

Loss of MFAP1 prevents chromosome alignment and causes a spindle assembly checkpoint-dependent mitotic arrest

To investigate the effect of MFAP1 loss on cell division, we first measured the duration of mitosis by tracking cells using bright-field microscopy. Control cells entered mitosis and underwent the metaphase-to-anaphase transition within 46 min on average (Fig 1B). Subsequently, control cells underwent cytokinesis and exited mitosis. In contrast, the majority of cells lacking MFAP1 remained arrested in mitosis for several hours before undergoing cell death or aberrantly exiting mitosis without attempting cytokinesis (Fig 1B). The increased duration of mitosis observed in cells depleted of MFAP1 was abrogated upon co-depletion of the spindle assembly checkpoint component Mad2 (Lara-Gonzalez *et al*, 2012) (Fig 1C). These results indicate that loss of MFAP1 causes a mitotic arrest that is dependent on the spindle assembly checkpoint.

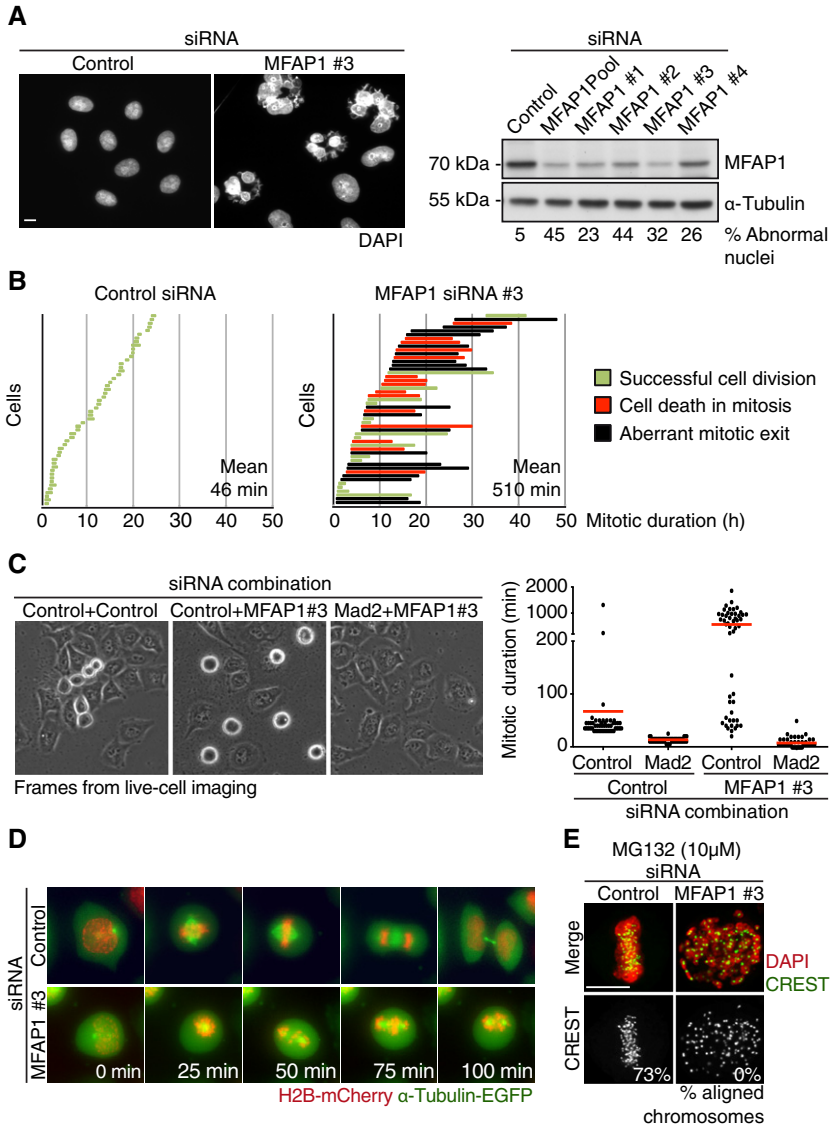

Figure 1. Depletion of MFAP1 causes a mitotic arrest and prevents chromosome alignment.

A Representative images of nuclear morphology (left) and immunoblot analysis of whole-cell extracts (right) of HeLa Kyoto cells 72 h after transfection with control siRNA or siRNA duplexes targeting MFAP1. Percentages of cells with abnormal nuclear morphology are indicated below the immunoblot (n > 200 cells, mean of three experiments).

B Mitotic duration and cell division outcome analysed by live imaging 32 h after the transfection with the indicated siRNA duplexes. Each bar represents the mitotic duration of a single cell (time from cell rounding to anaphase onset) (n = 50 cells).

C Selected frames from live-cell recording (left) and analysis of mitotic duration (right) of cells transfected with the indicated siRNA combinations for 32 h. Red bars mark the mean duration of mitosis (n = 50 cells).

D Live-cell imaging of cells stably co-expressing H2B-mCherry and α-tubulin-EGFP. Frames were recorded 24 h after transfection with control siRNA or siRNA targeting MFAP1. t = 0 min was set to the last frame before nuclear envelope breakdown.

E Immunofluorescence (IF) analysis of cells transfected with control or MFAP1 siRNA for 48 h and subsequently treated with 10 μM MG132 for 3 h. Percentage of cells with chromosome alignment is shown (n = 50 cells).

Data information: Scale bars, 10 μm.
Source data are available online for this figure.

The spindle assembly checkpoint dependency of the arrest in MFAP1-depleted cells suggested that chromosomes might fail to bi-orient on the mitotic spindle. To test this, we used live imaging of cells co-expressing histone H2B-mCherry and α-tubulin-EGFP. Control cells achieved chromosome alignment at the metaphase plate within an hour before initiating anaphase and exiting mitosis (8/9 cells) (Fig 1D). In contrast, cells lacking MFAP1 were unable to form a metaphase plate upon mitotic entry and remained arrested in mitosis with a scattered chromosome configuration (9/9 cells) (Fig 1D). To corroborate this observation, we treated cells with the proteasomal inhibitor MG132 that prevents anaphase onset and arrests cells in metaphase. Depletion of MFAP1 completely abolished

the chromosome alignment that was observed in the majority of control siRNA transfected cells after a 3-h arrest in MG132 (Fig 1E). These results indicate that MFAP1 is required for the alignment of chromosomes at the metaphase plate. This function of MFAP1 could contribute to the prometaphase arrest and mitotic catastrophe observed in cells lacking the protein.

MFAP1 is required for sister chromatid cohesion

A failure to align chromosomes could be caused by defects in mitotic spindle dynamics, kinetochore function or sister chromatid cohesion. Loss of sister chromatid cohesion prevents the stable attachment of microtubules to kinetochores and the bi-orientation of chromatids (Tanaka *et al*, 2000). We observed that centromeres in MFAP1-depleted prometaphase cells appeared to lack the pairwise arrangement normally found in control cells (Fig 1E). Therefore, we decided to test the status of sister chromatid cohesion in nocodazole-arrested mitotic cells by chromosome spreading. Chromosomes from control siRNA-transfected cells were connected at the central constriction reflecting intact cohesion between sister centromeres (Fig 2A). In contrast, the vast majority of chromosomes from MFAP1-depleted cells had lost their characteristic X shape and instead appeared as single chromatids (Fig 2A). Fluorescence *in situ* hybridization (FISH) experiments confirmed the loss of sister chromatid cohesion upon depletion of MFAP1 in intact mitotic cells (Fig 2B). These results suggest that MFAP1 is required for sister chromatid cohesion in mitosis. Remarkably, the severity of the sister chromatid cohesion loss phenotype in MFAP1-depleted cells was comparable to the loss of the centromeric cohesion protector SGOL1 (Fig 2A). To test whether loss of MFAP1 protein is responsible for the observed defects, we generated a cell line stably expressing a transgenic and siRNA-resistant version of MFAP1 that was tagged with AcGFP (*Aequora coerulescens* green fluorescent protein) and a FLAG epitope (AcFL-MFAP1-r) at a level close to the endogenous counterpart (Fig 2C, right panel). Expression of the RNAi-resistant transgene suppressed both the mitotic loss of sister chromatid cohesion and the interphase nuclear defect in cells transfected with the corresponding siRNA duplex targeting MFAP1 (Fig 2C). Thus, we have identified a role for the splicing factor MFAP1 in sister chromatid cohesion, the crucial connection between DNA copies that allows the bi-orientation and subsequent accurate segregation of chromosomes in mitosis.

A multitude of spliceosome components are required for sister chromatid cohesion in human cells

The requirement of MFAP1 for sister chromatid cohesion raised the question whether MFAP1 has a dedicated second role in cohesion independent of pre-mRNA splicing or whether there is a much more widespread requirement of spliceosome components for sister chromatid cohesion. Analysis of genome-wide RNAi screen data sets revealed an enrichment of spliceosome components in the category of genes whose depletion resulted in mitotic defects (Kittler *et al*, 2007; Hofmann *et al*, 2010; Neumann *et al*, 2010). A comparison of the proteomic composition of the human spliceosome (Zhou *et al*, 2002; Jurica & Moore, 2003) with genes classified as mitosis-defective in a genome-wide screen (Neumann *et al*, 2010) revealed an overlap of 33 factors. By transfecting siRNA pools and performing chromosome spreading analysis, we tested whether depletion of these 33 proteins had an effect on sister chromatid cohesion. Transfection of 26 siRNA pools targeting splicing genes resulted in a loss of sister chromatid cohesion in more than half of the cells (Fig 3A and B; for protein depletion data see Supplementary Fig S3A). Remarkably, siRNA pools targeting 18 splicing factors caused an almost complete disruption of sister chromatid cohesion that was comparable to the loss of SGOL1 or the loss of the core cohesin subunit SCC1 (Fig 3A and B). These included siRNA pools targeting SF3B1 (splicing factor 3B subunit 1), NHP2L1 (non-histone protein 2-like protein 1), SART1 (squamous cell carcinoma antigen recognized by T cells) and CDC5L (cell division cycle 5-like protein). Deconvolution experiments using individual siRNA duplexes for splicing factors whose siRNA pools caused the most severe defects in sister chromatid cohesion supported a causal relationship between loss of the target protein and the observed chromosomal phenotype (Supplementary Fig S2). Stable transgenic expression of tagged and RNAi-resistant versions of the spliceosome components NHP2L1 and SART1 fully restored sister chromatid cohesion in cells depleted of the endogenous counterparts (Fig 3C and Supplementary Fig S3B). Transfection of siRNA pools targeting MFAP1, NHP2L1 and SART1 also caused defects in sister chromatid cohesion in the human diploid colon carcinoma cell line HCT116 (Supplementary Fig S4) suggesting a general requirement of these splicing factors for cohesion in human cells.

Our observations demonstrate that the connection between pre-mRNA splicing and sister chromatid cohesion is not restricted to MFAP1 but extends well beyond. They suggest a widespread association of spliceosome component depletion with a loss of sister chromatid cohesion in human cells. Splicing proteins, whose depletion had a severe impact on sister chromatid cohesion, act in different subcomplexes and at different steps within the spliceosome assembly pathway (Supplementary Fig S5). SF3B1 is an essential component of the spliceosomal U2 snRNP complex and helps to target the complex to the branch point of introns in the initial phase of the splicing reaction (Wahl *et al*, 2009; Folco *et al*, 2011). NHP2L1 and SART1 are both components of the U5 and U4/U6 tri-snRNP complex, which associates with the spliceosome in a subsequent step (Makarova *et al*, 2001). CDC5L is a subunit of the Prp19 complex that is required for the activation of the spliceosome before the first step of the splicing reaction (Ajuh *et al*, 2000; Makarova *et al*, 2004; Grote *et al*, 2010). The fact that spliceosome components from distinct subcomplexes that act at different steps of spliceosome assembly are required for cohesion suggests that compromised pre-mRNA splicing in general could be responsible for the loss of sister chromatid cohesion. To investigate the link between splicing and sister chromatid cohesion, we decided to focus on the analysis of cells lacking the spliceosome components MFAP1, NHP2L1, SART1 and CDC5L.

Loss of spliceosome components disrupts sister chromatid cohesion in interphase

We first aimed to determine whether the loss of sister chromatid cohesion upon depletion of splicing factors occurred already during interphase or only upon entry into mitosis. To assess the status of sister chromatid cohesion in interphase, we used FISH probes for the *tff1* locus on chromosome 21 in post-replicative cells (Schmitz *et al*, 2007). Depletion of NHP2L1, SART1 and MFAP1 increased the

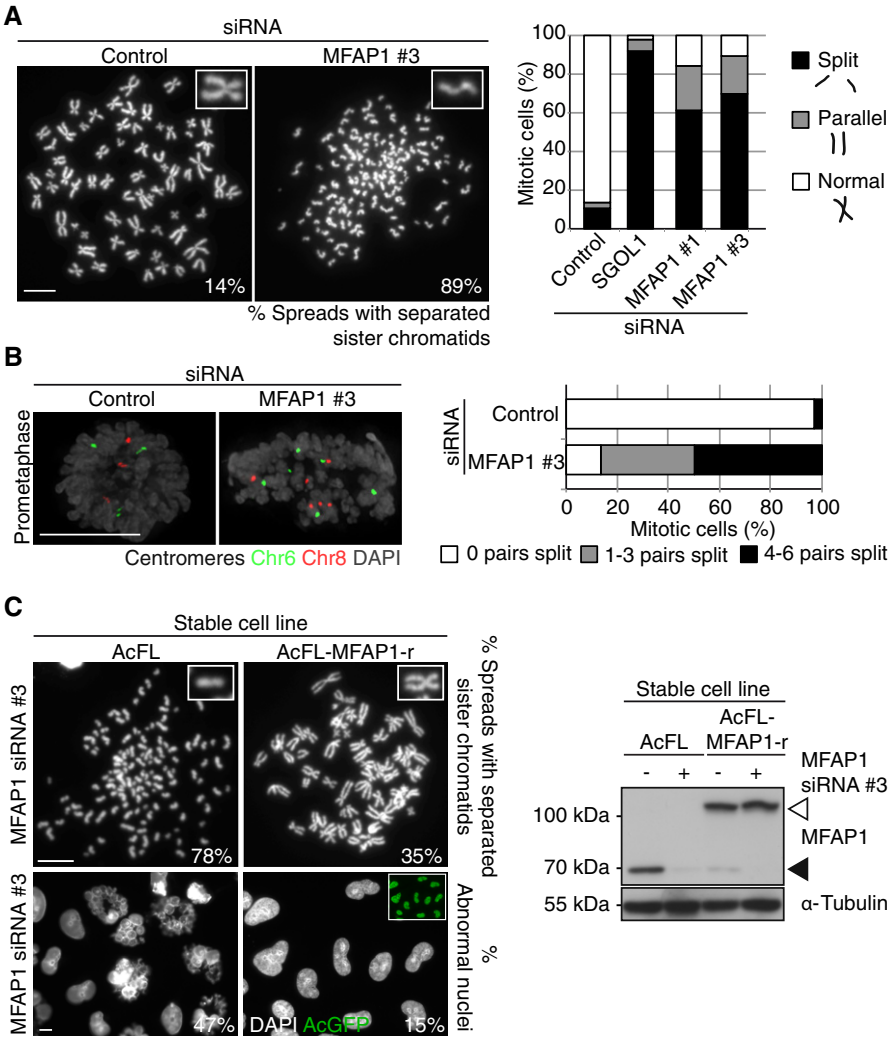

Figure 2. MFAP1 is required for sister chromatid cohesion in mitosis.

A Representative images of chromosome spreads (left) and quantification of the different states of sister chromatid cohesion (right) in cells that were transfected with the indicated siRNA duplexes 52 h prior to the analysis (n = 100 cells). Depletion of SGOL1 was used as a positive control for premature loss of sister chromatid cohesion.

B Fluorescence *in situ* hybridization (FISH) analysis performed using centromeric probes for chromosome 6 (green) and chromosome 8 (red) in cells transfected with the indicated siRNAs 48 h prior to analysis. Quantification of the number of centromere pairs that are more than 2 μm apart and were classified as split is shown (n > 30 cells).

C Chromosome spread analysis (52 h post-siRNA transfection) and IF analysis of interphase cells (72 h post-siRNA transfection) of cell lines stably expressing the AcFL tag alone or an siRNA-resistant version of MFAP1 (AcFL-MFAP1-r) following transfection with MFAP1 siRNA (left) (n > 100 cells, 3 experiments). Immunoblot of whole-cell extracts from the stable cell lines transfected with MFAP1 siRNA (+) or control siRNA (−) 72 h prior to analysis. Endogenous MFAP1 (filled arrowhead) and transgenic AcFL-MFAP1-r (open arrowhead) are indicated.

Data information: Scale bars, 10 μm.
Source data are available online for this figure.

distance between sister chromatid signals to a similar extent as depletion of sororin, a protein essential for sister chromatid cohesion in interphase (Rankin *et al*, 2005; Schmitz *et al*, 2007) (Fig 4A). In contrast, loss of SGOL1, a protein essential only for maintaining centromeric cohesion upon entry into mitosis (Salic *et al*, 2004; McGuinness *et al*, 2005), did not alter the distance between sister chromatid signals (Fig 4A). These results indicate that the loss of splicing factors disrupts sister chromatid cohesion in interphase. This defect could then result and culminate in the emergence of single chromatids in mitotic chromosome spreads.

Spliceosome components are dispensable for cohesin loading onto chromatin and SMC3 acetylation

To define the molecular mechanism that underlies the link between splicing and sister chromatid cohesion, we scrutinized the properties of cohesin components in interphase nuclei. To interrogate the loading of cohesin onto chromatin, we quantified the signal intensity of extraction-resistant SCC1 staining in fixed interphase nuclei (Schmitz *et al*, 2007). To facilitate comparative analysis and provide an internal experimental standard, we mixed untreated cells that

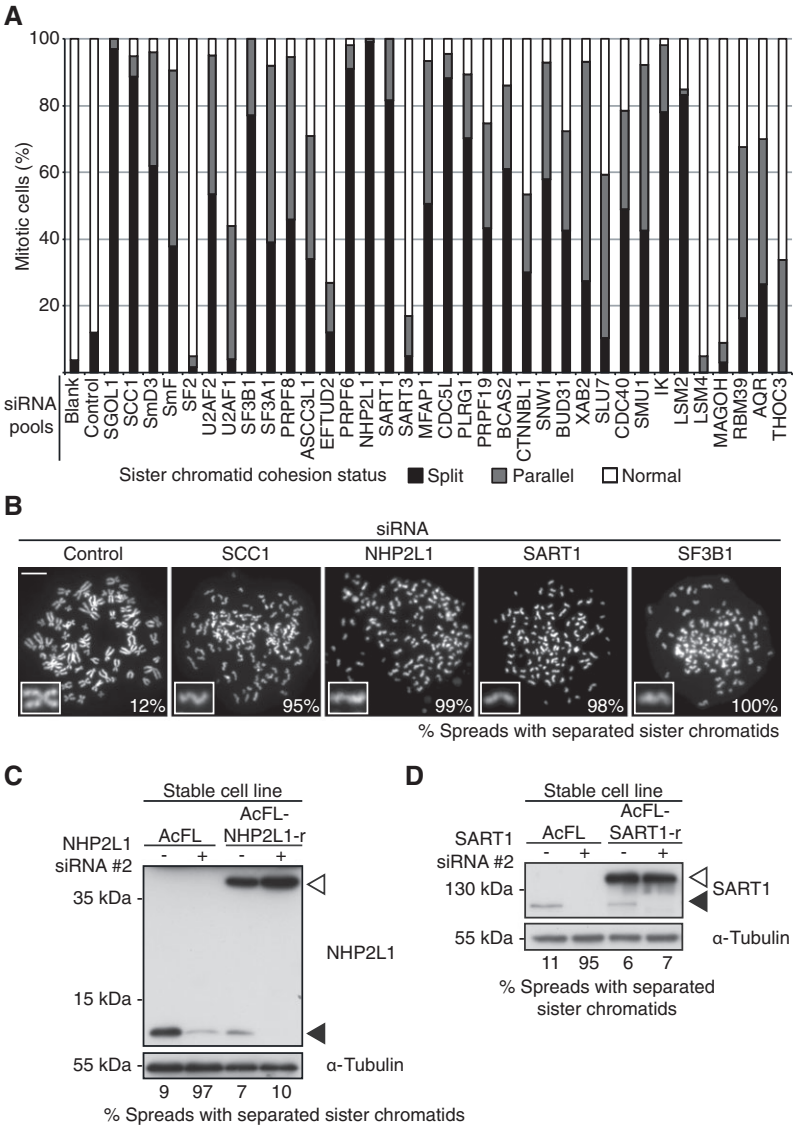

Figure 3. Identification of spliceosome components that are required for sister chromatid cohesion.

A Status of sister chromatid cohesion in HeLa Kyoto cells transfected with siRNA pools targeting the indicated spliceosome components 52 h before analysis (n = 100 cells). Cohesion status was determined by chromosome spreading.

B Chromosome spread images corresponding to the data shown in (A). Scale bar, 10 μm.

C Immunoblot analysis of whole-cell extracts prepared from cell lines stably expressing the AcFL tag or an siRNA-resistant NHP2L1 (AcFL-NHP2L1-r). Extracts were prepared 72 h after transfection with control (−) or NHP2L1 siRNA. Endogenous NHP2L1 (filled arrowhead) and transgenic AcFL-NHP2L1-r (open arrowhead) are indicated. Percentages of cells exhibiting loss of sister chromatid cohesion are indicated (n = 100 cells each, mean of three independent experiments).

D Transgenic cell lines stably expressing AcFL or an siRNA-resistant version of SART1 (AcFL-SART1-r) were transfected with control (−) and SART1 siRNA (+) and analysed as in (C).

Source data are available online for this figure.

were labelled with H2B-mCherry and unlabelled cells that were transfected with siRNA duplexes. Although depletion of the cohesin-loading factor SCC4 (Ciosk *et al*, 2000; Watrin *et al*, 2006) reduced the intensity of extraction-resistant SCC1, depletion of the splicing proteins NHP2L1, MFAP1 and SART1 had no discernible effect (Fig 4B). Thus, loss of spliceosome components does not interfere with the bulk loading of cohesin onto chromatin in interphase cells.

Acetylation of the core cohesin subunit SMC3 acts as a marker for the establishment of sister chromatid cohesion during DNA replication (Rolef Ben-Shahar *et al*, 2008; Unal *et al*, 2008; Zhang *et al*, 2008; Rowland *et al*, 2009; Nishiyama *et al*, 2010). Depletion of the spliceosome components NHP2L1, MFAP1, SART1 and CDC5L caused a minor reduction of SMC3 acetylation in replicating cells (Fig 4C). In contrast, loss of the acetyltransferases ESCO1 and ESCO2 (Hou & Zou, 2005) largely abolished SMC3 acetylation (Fig 4C). The minor reduction of SMC3 modification cannot explain the dramatic loss of sister chromatid cohesion detected in cells lacking splicing components. Even the sevenfold reduction in

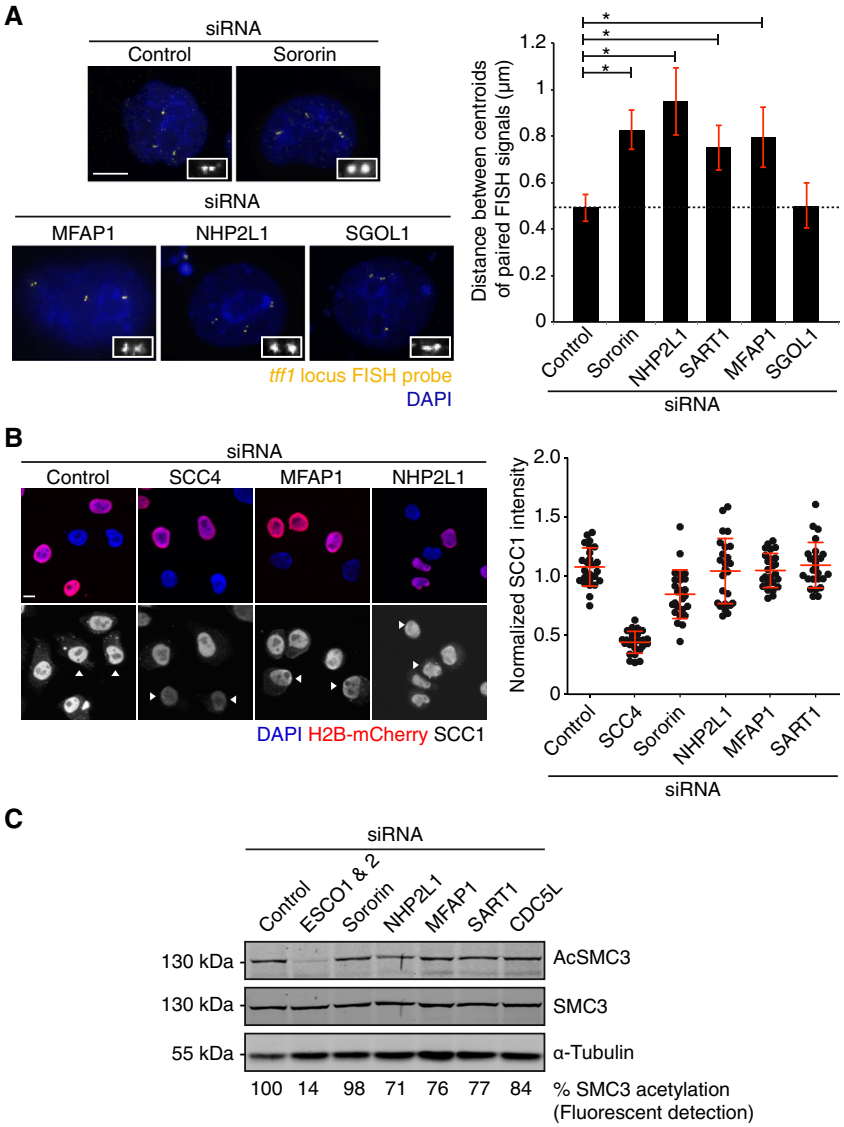

Figure 4. Depletion of splicing factors abrogates sister chromatid cohesion in interphase despite cohesin loading and SMC3 acetylation.

A Interphase FISH of G2 synchronized HeLa Kyoto cells that were transfected with control siRNA or siRNA duplexes targeting MFAP1 (53 h prior to analysis), sororin, SGOL1 or NHP2L1 (29 h prior to analysis). FISH was performed with a probe specific for the *tff1* locus on trisomic chromosome 21 (yellow). DNA was stained with DAPI (blue). Magnified images of single pairs of FISH signals are displayed in the insets. Graph depicts the distance between the paired FISH signals measured in each of the indicated siRNA treatments. Bars represent mean ± SEM. Asterisks indicate a significant difference according to Student's *t*-test ($P < 0.05$) ($n = 30$ paired signals). Scale bar, 10 µm.

B IF analysis of extraction-resistant SCC1 in H2B-mCherry-expressing cells that were untreated or in mCherry-negative cells that were transfected with the indicated siRNA duplexes (white arrowheads). Graph shows SCC1 fluorescence intensity quantification normalized to DAPI intensity and expressed as ratio between untransfected and siRNA transfected cells. Bars represent mean ± SD ($n > 25$ cells). Scale bar, 10 µm.

C Immunoblot analysis of whole-cell extracts from S phase synchronized cells that were previously transfected with sororin or NHP2L1 siRNAs (for 33 h) or control, MFAP1, SART1 or CDC5L siRNAs (for 51 h). The ratio of SMC3 acetylated at Lys105 and Lys106 (AcSMC3), and total SMC3 was measured by fluorescent detection and normalized to the ratio determined for cells that were transfected with control siRNA. α-tubulin serves as a loading control.

Source data are available online for this figure.

SMC3 acetylation observed in cells co-depleted of ESCO1 and ESCO2 is not associated with a comparably penetrant disruption of cohesion (data not shown). Our results indicate that cells lacking spliceosome components lose sister chromatid cohesion during interphase despite loading cohesin onto chromatin and the occurrence of SMC3 acetylation, an indicator for cohesion establishment.

Spliceosome components are required for the stable association of cohesin with chromatin in G2 cells

Following DNA replication, a subpopulation of cohesin complexes binds to chromatin with a mean residence time of around 6 h (Gerlich *et al*, 2006). This stably associated pool requires the protein sororin (Schmitz *et al*, 2007) and is thought to provide the

long-lived links mediating cohesion from S phase into mitosis. Our observation that the loss of splicing factors disrupts sister chromatid cohesion in G2 phase raises the possibility that the dynamics of cohesin association with chromatin are altered. To test this possibility, we used fluorescence recovery after photobleaching (FRAP) experiments. Cells stably expressing SMC1-EGFP were released from an S phase arrest for 5 h to allow entry into G2 phase. Following photobleaching of SMC1-EGFP in one half of the nucleus, the loss of the fluorescent signal in the unbleached nuclear area and the recovery of the signal in the bleached nuclear area were measured over 120 min (Fig 5). The redistribution kinetics of chromatin-bound cohesin were analysed by plotting the intensity difference between the two areas over time. Consistent with published observations (Gerlich *et al*, 2006; Schmitz *et al*, 2007), the SMC1-EGFP intensity difference dropped slowly and persisted until 120 min after photobleaching in control siRNA transfected cells (Fig 5). In contrast, in cells transfected with siRNA duplexes targeting the splicing proteins MFAP1, CDC5L and SART1, the intensity difference decreased rapidly and the fluorescence in the bleached and unbleached area equilibrated within about 45 min (Fig 5). Depletion of spliceosome components had a similar effect on cohesin dynamics as loss of sororin, a protein that antagonizes the activity of the cohesin release mechanism (Nishiyama *et al*, 2010) (Fig 5). Our results suggest that cohesin complexes dissociate from chromatin faster in cells lacking spliceosome components than in control cells. It is thus possible that splicing factors contribute to sister chromatid cohesion by

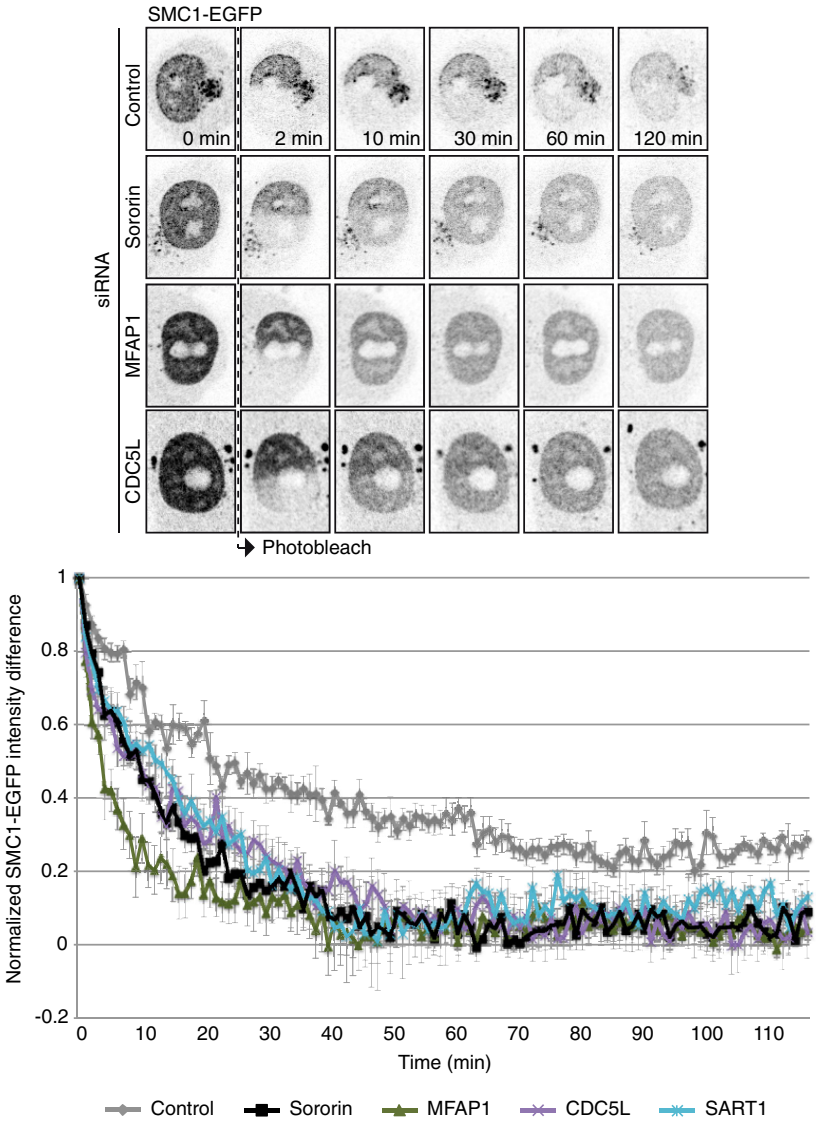

Figure 5. Stable association of cohesin with chromatin requires splicing factors.
Representative frames from fluorescence recovery after photobleaching (FRAP) experiments in SMC1-EGFP-expressing cells that were synchronized in G2 and that were previously transfected with control, MFAP1, SART1 and CDC5L siRNA duplexes (for 53 h) or with control and sororin siRNA (for 29 h) (upper panel). The graph shows the difference between SMC1-EGFP fluorescence intensity in the unbleached area and the intensity in the bleached area of the nucleus normalized to the first post-bleach frame and plotted over time (lower panel). Bars represent mean ± SEM, $n = 6$ cells for each condition from two independent experiments.

ensuring the stable association of cohesin with chromatin. Failure to do so may explain why cells that lack spliceosome subunits lose sister chromatid cohesion soon after DNA replication.

Expression of RNase H1 does not restore cohesion in splicing factor-depleted cells

Next, we investigated the molecular basis for how depletion of splicing factors perturbed the stable association of cohesin with chromatin and sister chromatid cohesion. Defective splicing of pre-mRNAs could abrogate sister chromatid cohesion through the formation of R loops, DNA:RNA hybrid structures that can threaten genome stability (Li & Manley, 2005; Aguilera & Garcia-Muse, 2012). To test this possibility, we generated a cell line overexpressing RNase H1, an enzyme that cleaves the RNA moiety of DNA:RNA hybrids (Cerritelli & Crouch, 2009; Skourti-Stathaki *et al*, 2011). Expression of nuclear-targeted RNase H1-EGFP failed to restore sister chromatid cohesion upon depletion of spliceosome components (Supplementary Fig S6) indicating that R loops are not responsible for the loss of cohesion.

Loss of spliceosome components reduces the protein level and impairs the splicing of sororin but not of core cohesin subunits

Alternatively, we hypothesized that compromised splicing and defective pre-mRNA processing could lead to the acute loss of one or multiple proteins that are essential for sister chromatid cohesion. Profiling of protein levels of cohesin subunits or regulators revealed that splicing factor depletion did not severely reduce the steady-state abundance of the cohesin subunits SMC1, SMC3, SCC1 and SA2 (Fig 6A). In contrast, depletion of all splicing factors tested (NHP2L1, MFAP1, SART1 and CDC5L) resulted in a fourfold or higher drop in the protein levels of sororin, a protein required for maintenance of cohesion through S–G2 phase into mitosis and for the stable association of cohesin with chromatin (Fig 6A). The loss of spliceosome components could compromise the splicing of sororin pre-mRNA and, as a consequence, the abundance of mature sororin protein. Consistent with this hypothesis, analysis of the presence of exon–intron junctions in sororin RNA by real-time PCR indicated the increased retention of intron 1 and 2 in cells depleted of splicing factors (Fig 6B). In contrast, depletion of spliceosome subunits only had minor effects on the retention of introns in the RNAs encoding core cohesin subunits (Fig 6B). Retention of intron 1 in sororin's mRNA would cause a translational frame shift after the coding exon 1 generating a stop codon in exon 3 or intron 2 if the latter is not removed. The resulting truncated protein would only contain the 15 N-terminal amino acids corresponding to the sequence of sororin and would be non-functional.

Defects in pre-mRNA splicing could reduce protein levels acutely especially when coupled to a reduced half-life of the corresponding mRNA and/or protein. To assess the stability of sororin mRNA, we treated cells with actinomycin D to inhibit transcription. Sororin mRNA displayed reduced stability compared to the mRNAs encoding core cohesin subunits and to the mRNA encoding glyceraldehyde 3-phosphate dehydrogenase (GAPDH) (Supplementary Fig S7A). In contrast to core cohesin subunits, sororin protein abundance dropped to about 25% within 2 h after releasing cells from mitosis into the G1 phase of the cell cycle (Fig 6C, left panel; for fluorescent quantification see Supplementary Fig S7B). The reduction in sororin protein level was further enhanced by treatment of cells with the protein synthesis inhibitor cycloheximide (Fig 6C, right panel; Supplementary Fig S7B). Thus, consistent with sororin being a substrate of the anaphase-promoting complex/cyclosome (APC/C) (Rankin *et al*, 2005), the protein is highly unstable in G1 cells.

Altogether, our observations raise the possibility that the loss of splicing machinery components impacts on sister chromatid cohesion by compromising the splicing of sororin pre-mRNA and, as a consequence, perturbing the cellular level of mature sororin protein. Consistent with this hypothesis, the loss of sororin and the depletion of splicing factors have similar phenotypic consequences: the loss of sister chromatid cohesion during interphase and the failure of cohesin to stably associate with chromatin.

Expression of an intronless version of sororin restores sister chromatid cohesion in cells lacking splicing factors

To test the hypothesis that failure of sororin pre-mRNA processing is causally linked to the loss of cohesion in cells depleted of spliceosome subunits, we generated a cell line stably expressing an intronless version of sororin (Fig 7A). The AcFL-tagged transgene (AcFL-Sororin-r) was also rendered resistant to sororin siRNA. Expression of AcFL-Sororin-r fully suppressed the loss of sister chromatid cohesion observed upon depletion of endogenous sororin suggesting that the transgene was functional (Fig 7A). Importantly, the intronless sororin transgene also potently restored sister chromatid cohesion in cells depleted of the splicing factors MFAP1, NHP2L1, SART1 and CDC5L (Fig 7B and C). In contrast, expression of AcFL-Sororin-r only had a minor effect in cells depleted of the core cohesin subunit SCC1 or the centromeric protector protein SGOL1 indicating that the transgene cannot efficiently compensate for loss of core cohesin functions (Fig 7C). These results suggest that the defective synthesis of mature sororin protein makes a major contribution to the loss of sister chromatid cohesion in cells lacking spliceosome subunits (Fig 8B). Expression of the intronless sororin transgene did not, however, restore mitotic progression in cells transfected with siRNAs targeting spliceosome subunits indicating that the lack of as yet unidentified additional factors also contributes to the mitotic arrest in those cells (Supplementary Fig S8A).

The loss of sister chromatid cohesion upon depletion of spliceosome subunits requires the anti-establishment factor WAPL

Sororin ensures the stable association of cohesin with chromatin in interphase by antagonizing the activity of the cohesin release protein WAPL (Nishiyama *et al*, 2010). If defective splicing disrupts cohesin's binding to chromatin and thereby sister chromatid cohesion through compromising sororin function, loss of WAPL should restore the links between sister chromatids in cells lacking spliceosome components. Indeed, we found that depletion of WAPL strongly suppressed the sister chromatid cohesion defect not only in cells depleted of sororin but also in cells transfected with siRNA duplexes targeting the splicing factors MFAP1, NHP2L1, SART1 and CDC5L (Fig 8A; for protein depletion data see Supplementary Fig S8B). This observation supports the conclusion that spliceosome factors contribute to sister chromatid cohesion largely by maintaining sororin function, which counteracts the cohesin releasing activity of WAPL (Fig 8B).

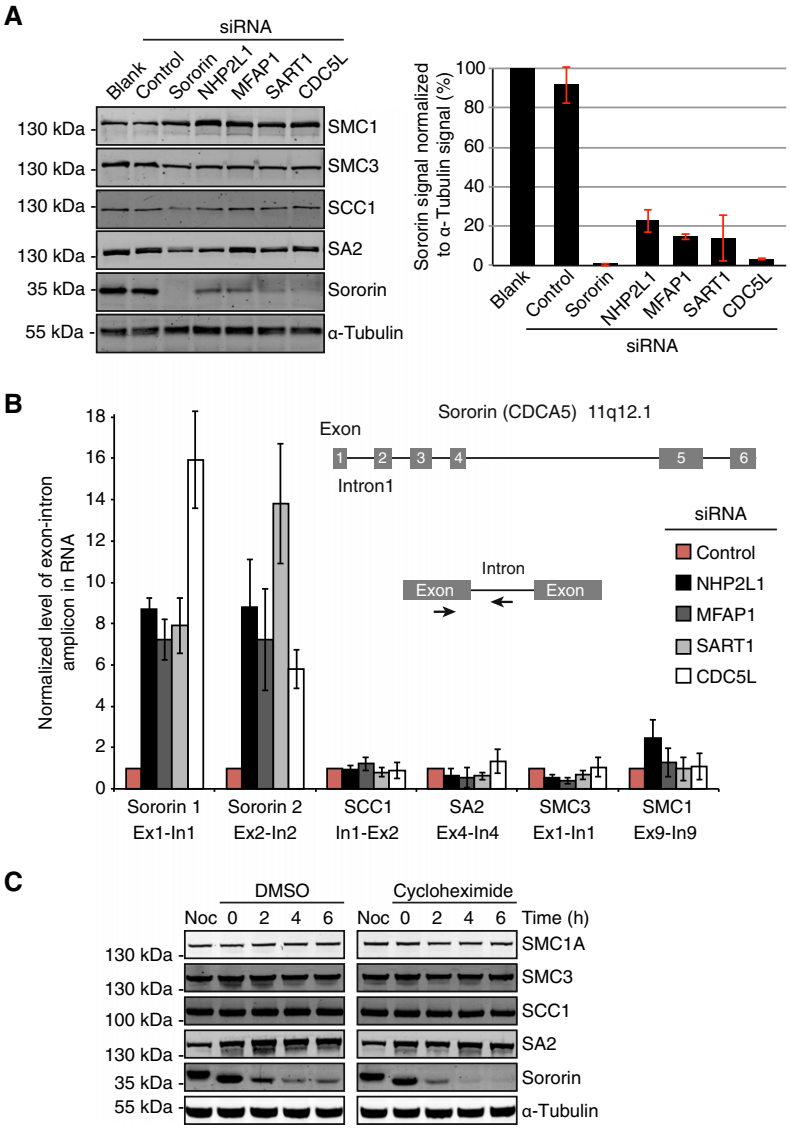

Figure 6. Loss of spliceosome components reduces sororin protein level and compromises sororin pre-mRNA processing.

A Immunoblots from whole-cell extracts (left) of G2 synchronized cells that were previously transfected with no siRNA (blank), control, MFAP1, SART1 or CDC5L (for 53 h), sororin or NHP2L1 (for 29 h) siRNA duplexes. Fluorescent detection was used to measure the intensity of sororin signal relative to α-tubulin signal (right). The resulting ratios were normalized to the ratio observed in untreated cells. Graph displays the mean ratios of two experiments (errors bars represent SD).

B Schematic representation of the genomic locus of human sororin (upper illustration). Primer position (lower illustration) for the analysis of intron retention by real-time quantitative PCR (RT-qPCR). Quantification of the levels of exon-intron amplicons in the RNA of cohesin genes (graph). RNA isolated from G2 synchronized cells that were transfected with control, MFAP1, SART1, CDC5L siRNAs (for 53 h), sororin or NHP2L1 siRNAs (for 29 h) was used for the analysis. Intron retention in cohesin genes was determined by RT-qPCR analysis using primer pairs that amplify across a specific intron–exon junction (as indicated). Intron–exon amplicon values were normalized to intra-exon amplicon values for each gene (see Materials and Methods). The quantification was performed using the $\Delta\Delta C_t$ method (Winer *et al*, 1999). The ratio obtained in control siRNA transfected cells was set to 1. The graph displays the mean of three independent experiments (errors bars represent SD).

C Immunoblots of whole-cell extracts prepared from cells that were released from a nocodazole arrest (Noc) for the indicated times in the presence of dimethyl sulfoxide (DMSO) solvent or the protein translation inhibitor cycloheximide (100 μg/ml).

Source data are available online for this figure.

Discussion

Cohesin and sister chromatid cohesion lie at the heart of chromosome biology. They are required for chromosome segregation, DNA repair, chromosome structure and gene regulation. Using a functional genomic approach, we have defined a requirement of pre-mRNA splicing factors for sister chromatid cohesion in human cells. Depletion of a multitude of splicing factors by RNAi abrogated the stable association of cohesin with chromatin after DNA replication and culminated in a dramatic loss of sister chromatid cohesion upon mitotic entry. The fact that we detected a severe loss of sister chromatid cohesion upon depletion of more than 26 spliceosome subunits suggests that defects in pre-mRNA splicing itself or in the processing of one or multiple transcripts are causally linked to the

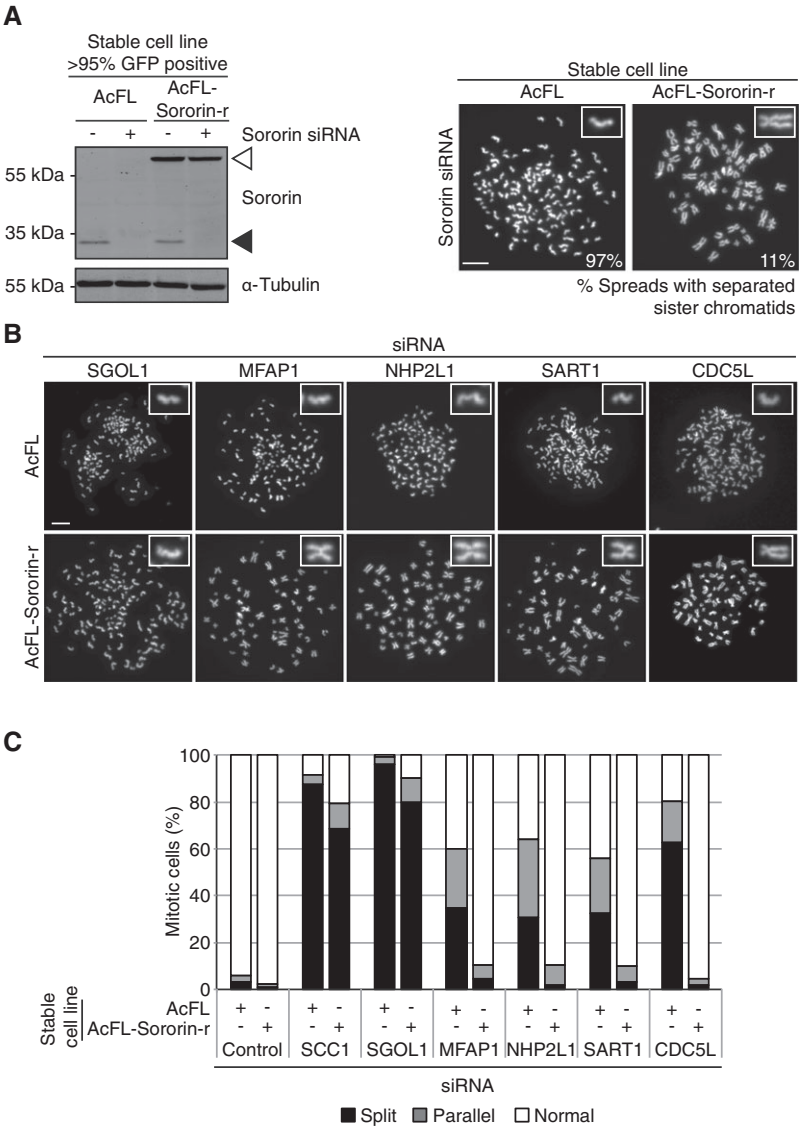

Figure 7. Expression of an intronless construct of sororin suppresses the loss of cohesion caused by depletion of splicing factors.

A Immunoblot analysis of sororin protein levels in whole-cell extracts prepared from cells stably expressing either the AcFL tag or an AcFL-tagged intronless and siRNA-resistant transgene of sororin (AcFL-sororin-r). Cells were transfected with sororin (+) or control (−) siRNA duplexes 72 h prior to analysis (left). The endogenous protein (filled arrowheads) and the transgenic AcFL-sororin-r counterpart (open arrowheads) are indicated. Chromosome spreads (right) from the indicated cell lines were prepared 28 h after transfection with sororin siRNA (n > 100 cells, mean from 3 experiments). Scale bar, 10 μm.

B Representative images of chromosome spreads from the indicated cell lines transfected with SGOL1, NHP2L1 (34 h), control, MFAP1, SART1 (40 h) or CDC5L (56 h) siRNA duplexes. Scale bar, 10 μm.

C Quantification of sister chromatid cohesion status corresponding to the experiment described in (B) (n > 100 cells, mean of 3 experiments). SCC1 siRNA was transfected 56 h prior to analysis.

Source data are available online for this figure.

observed chromosomal phenotype. At this point, we have no evidence that would support a direct involvement of spliceosome components in cohesion.

Pre-mRNA splicing is an essential process for gene expression in eukaryotes (Braunschweig *et al*, 2013). Accordingly, we found that depletion of spliceosome subunits causes cell lethality as a terminal phenotype (data not shown). However, our analysis suggests that an enhanced turnover of cohesin on interphase chromatin followed by a cell cycle arrest in mitosis with split sister chromatids is an early cellular consequence of compromising splicing. This suggests that sister chromatid cohesion is highly sensitive to pre-mRNA splicing defects. Furthermore, it provides a potential explanation for the prominent identification of spliceosome components as mitosis-defective hits in reverse genetic screens (Kittler *et al*, 2007; Hofmann *et al*, 2010; Neumann *et al*, 2010).

Our experiments indicate that compromised splicing leads to defects in sister chromatid cohesion largely through the loss of sororin function, thus providing a molecular explanation for the essential

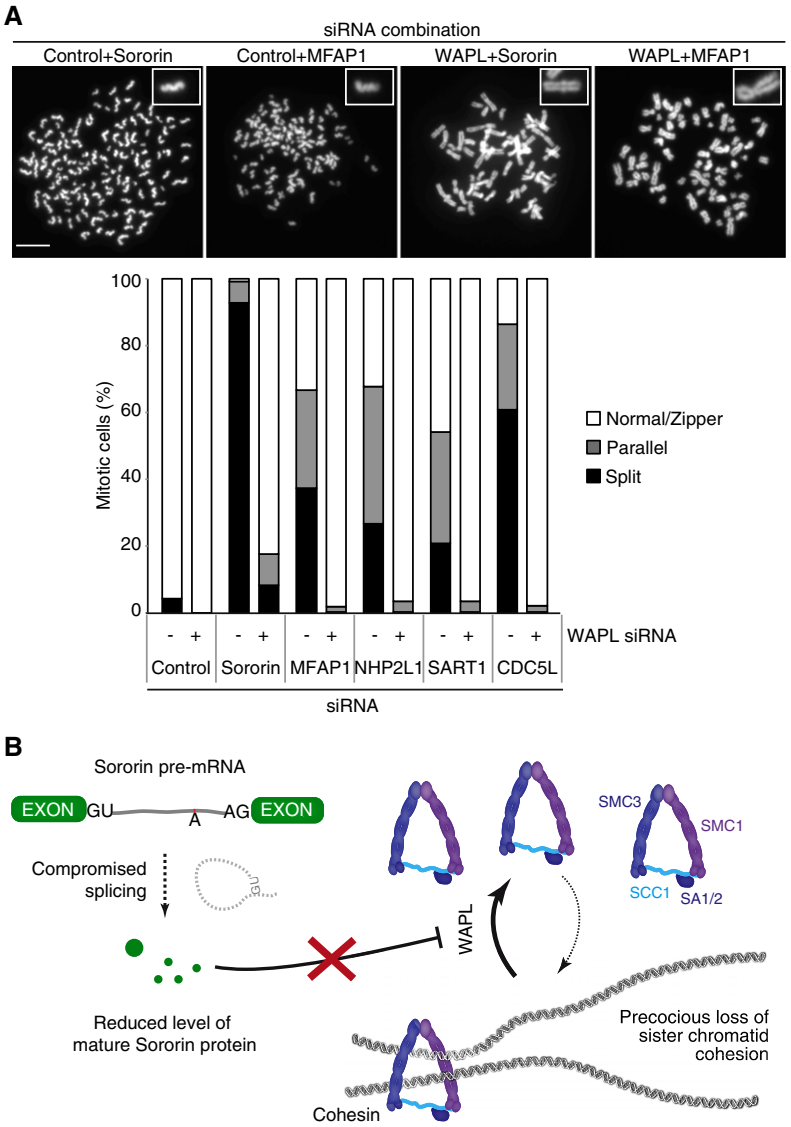

Figure 8. The loss of sister chromatid cohesion caused by depletion of spliceosome subunits depends on WAPL.

A HeLa Kyoto cells were co-transfected with control or WAPL siRNA duplexes and siRNA duplexes targeting sororin, MFAP1, NHP2L1, SART1 or CDC5L. Cells were transfected with control or WAPL siRNA 32 h before transfection of the second siRNA duplex. Chromosome spreads were prepared 66 h (for sororin and NHP2L1), 72 h (for MFAP1 and SART1) or 88 h (for CDC5L) after the first transfection. Representative chromosome spread images (upper panel). Scale bar, 10 μm. Quantification of sister chromatid cohesion status (lower panel). Graph displays the mean values of two independent experiments ($n > 100$ cells each).

B Model. Compromised splicing reduces the level of sororin protein. The unrestrained cohesin release activity of WAPL could then promote the enhanced dissociation of cohesin from chromatin and, as a consequence, abrogate sister chromatid cohesion.

role of splicing factors in mitosis (Fig 8B). Several lines of experimental evidence support this conclusion. Loss of sororin and loss of splicing factors share a phenotypic signature (Schmitz *et al*, 2007): failure of cohesin to stably associate with chromatin and defects in sister chromatid cohesion in post-replicative interphase cells despite cohesin loading and SMC3 acetylation. Furthermore, we detected aberrant processing of sororin pre-mRNA and reduced sororin protein levels in cells depleted of splicing factors. Lastly, expression of an intronless version of sororin and depletion of the cohesin release protein WAPL, whose activity is antagonized by sororin, were both able to suppress the sister chromatid cohesion defect observed in cells lacking spliceosome components. These rescue experiments also indicate that the unrestrained WAPL-induced dissociation of cohesin from chromatin in interphase might be responsible for the loss of cohesion observed in mitotic cells upon depletion of splicing factors. While we describe 26 splicing factors whose depletion severely compromises sister chromatid cohesion, we analysed the effects of depletion of four proteins, MFAP1, NHP2L1, SART1 and CDC5L, in detail. Based on the phenotypic similarity caused by depletion of these 4 components, it is tempting to speculate that compromised sororin function may underlie the loss of sister chromatin cohesion elicited by depletion of most if not all splicing factors described here. This extrapolation is supported by the analysis and global RNA profiling of cells lacking the splicing factor SNW1 (Zhou

et al, 2002; see van der Lelij *et al*, 2014), a protein also identified in our screen for spliceosome components that are required for cohesion. Based on our results, it is conceivable that compromised processing of sororin mRNA and the ensuing loss of cohesion might also contribute to the mitotic defects previously reported in human cells depleted of factors linked to RNA metabolism, such as the TREX helicase UAP56, the RNA-binding protein RBMX, the splicing protein SON and the Prp19 splicing complex (Huen *et al*, 2010; Yamazaki *et al*, 2010; Matsunaga *et al*, 2012; Hofmann *et al*, 2013).

Our results support the notion that sister chromatid cohesion in human cells is exquisitely sensitive to the dosage of sororin protein. This highlights the delicate balance that cells have to strike between the activity of the cohesin release factor WAPL and the sororin-dependent mechanism that counteracts WAPL and promotes the establishment of long-lived connections between sister chromatids. This balancing act is presumably necessitated by the important roles of cohesin dissociation from chromatin. WAPL-dependent cohesin release from mitotic chromosome arms drives the formation of the iconic X shape of chromosomes and facilitates the correct partitioning of sister genomes during anaphase (Kueng *et al*, 2006; Haarhuis *et al*, 2013; Tedeschi *et al*, 2013). It also spares a soluble pool of the cohesin complex from cleavage by separase at the metaphase-to-anaphase transition providing a ready supply of intact cohesin complexes that can be loaded onto chromatin during telophase/G1 to control chromatin structure and gene regulation (Wendt *et al*, 2008; Hadjur *et al*, 2009; Nativio *et al*, 2009; Sofueva *et al*, 2013; Tedeschi *et al*, 2013). Lastly, WAPL-mediated release of cohesin from DNA prevents chromatin condensation in interphase cells (Tedeschi *et al*, 2013).

Although we cannot rule out that defective processing of other transcripts also impairs cohesion in splicing factor-depleted cells, defective sororin function appears to be the major contributing factor. In contrast to other cohesin proteins, sororin is degraded at the end of the cell cycle through APC/C-mediated proteasomal degradation (Rankin *et al*, 2005) thereby necessitating renewed sororin translation from processed mRNA for every ensuing S phase. We hypothesize that this could render sister chromatid cohesion vulnerable to defects in pre-mRNA splicing. The reduced half-life of sororin mRNA and protein is likely to accelerate the conversion of splicing defects into a reduction of mature protein. Our data suggest that the removal of introns from sororin pre-mRNA may have a particularly strict requirement for intact spliceosomes. While this strict requirement may not be unique to sororin pre-mRNA on a transcriptome-wide basis (see van der Lelij *et al*, 2014), sororin appears to be the most sensitive pre-mRNA to depletion of spliceosome components amongst essential cohesin factors. This sensitivity may act synergistically with the high turnover of sororin gene products to cause a reduction of sororin protein level and a resulting defect in sister chromatid cohesion. The molecular basis for a potentially selective dependency of sororin pre-mRNA splicing (and that of some other pre-mRNAs) on intact spliceosomes remains to be determined. Its elucidation will be facilitated by the transcriptome-wide mapping of spliceosome assembly and branch site usage in conjunction with the global analysis of intron retention following loss of particular spliceosome components.

There is precedence for a specific mitotic defect caused by compromised splicing of a transcript in budding yeast. Removal of the intron from the gene encoding α-tubulin alleviated the mitotic arrest in cells that harboured spliceosome mutations (Burns *et al*, 2002). Expression of an intronless allele of sororin restored sister chromatid cohesion but did not alleviate the mitotic block in human cells depleted of splicing components. This suggests that the defective processing of additional transcripts may contribute to the spindle assembly checkpoint-mediated arrest that we observed in cells lacking splicing factors.

We noted that the efficiency of cohesion rescue by expression of an intronless sororin transgene was reduced if cells lacking spliceosome components were analysed at later time points. This suggests that cohesion fatigue, the gradual loss of cohesion in mitotically arrested cells (Daum *et al*, 2011; Stevens *et al*, 2011), contributes to the observed sister chromatid cohesion in cells lacking spliceosome components. However, our results indicate that a defect in sororin function rather than cohesion fatigue caused by a protracted mitotic arrest is the major cause for the disruption of cohesion in cells depleted of splicing factors. Firstly, splicing factors are required for the stable association of cohesin with chromatin during interphase. Second, depletion of splicing factors abrogates cohesion prior to mitotic entry. Lastly, expression of an intronless sororin transgene and the depletion of WAPL efficiently suppresses the loss of sister chromatid cohesion elicited by depletion of spliceosome subunits.

The phenotypic link between splicing and sister chromatid cohesion that we describe here may have biomedical implications. One of the splicing factors whose depletion by siRNA causes a dramatic loss of cohesion is SF3B1. *SF3B1* has recently emerged as one of the most frequently mutated genes in patients with chronic lymphocytic leukaemia (CLL) (Rossi *et al*, 2011; Wang *et al*, 2011; Quesada *et al*, 2012). Somatic *SF3B1* mutations were also detected at high frequency in myelodysplastic syndrome (MDS) patients (Papaemmanuil *et al*, 2011; Yoshida *et al*, 2011). The recurrent nature of *SF3B1* mutations in MDS and CLL suggests that they act as key drivers in hematopoietic proliferative disorders. SF3B1 is an essential component of the spliceosomal U2 snRNP (Wahl *et al*, 2009; Folco *et al*, 2011). *SF3B1* mutations could drive dysplasia and malignancy by altering the splicing pattern of oncogenes or tumour suppressors (Gentien *et al*, 2014). Our findings raise the possibility that heterozygous *SF3B1* mutations detected in CLL and MDS cells could contribute to pathology also by altering the turnover of cohesin on chromatin, and hence affecting chromosome stability, DNA repair and gene regulation.

Materials and Methods

Cells and growth conditions

HeLa Kyoto, HEK 293FT and HCT116 cells used in this study were grown in Dulbecco's modified Eagle medium, DMEM (Invitrogen) supplemented with 10% FCS (Sigma) and 1% PenStrep (Invitrogen). In order to establish stable cell lines, media supplemented with either 0.35 μg/ml puromycin (Sigma) or 500 μg/ml G418 (Invitrogen) were used. Cells were grown in an incubator that was maintained at 37°C with 5% CO_2.

siRNA screen

To compile a list of candidate genes, we selected 851 genes that were either identified as causing mitotic failure upon depletion according

to the genome-wide or targeted functional genomic screens (Mukherji *et al*, 2006; Kittler *et al*, 2007; Conery & Harlow, 2010; Neumann *et al*, 2010) or gene products that were identified as midbody-associated by proteomic analysis (Skop *et al*, 2004). Subsequently, we eliminated genes that were either well-characterized regulators of cell division, pseudogenes, ribosomal proteins or annotation errors according to NCBI databases. Based on this winnowing process, we compiled a final candidate list of 718 genes that were targeted in the primary screen. Dharmacon siGENOME smartpool siRNAs (0.1 nmol) were obtained for the 718 genes in 96-well plate format. Each well contained a pool of 4 siRNAs targeting a single gene. Positive controls (known mitotic regulators such as ECT2, MgcRacGAP, AURKB) and non-targeting negative controls (scrambled siRNA and RISC free siRNA) were included as well. Prior to cell seeding, siRNA pools (final concentration 37.5 nM) and the transfection reagent [Lipofectamine RNAiMAX (Invitrogen) at 0.167 μl/well at a final siRNA to RNAiMAX ratio of 1:600] were deposited in the wells [clear-bottomed 96-well plates (Falcon, Beckton Dickinson)] and mixed. Subsequently, 2,500 HeLa Kyoto cells were added to each well. Cells were grown for 52 h at 37°C and 5% CO_2 in DMEM and then processed for fixation with ethanol at −20°C overnight. Following the fixation, the cells were stained with Cellomics Whole Cell Stain (1:75 dilution, Thermo Scientific), and the DNA was visualized by DAPI (4′,6-diamidino-2-phenylindole dihydrochloride, Invitrogen) at a final concentration of 1 μg/ml. The screen was performed in triplicate. Automated image acquisition was performed using an ArrayScan ATI microscope (Thermo Scientific) equipped with a 10× objective. Twenty images per well were captured and subsequently processed using ImageJ software (http://rsbweb.nih.gov/ij/). The processed images were scored for the percentage of cells containing abnormally shaped nuclei (fragmented, multilobed nuclei) or multiple nuclei. The three biological plates were scored independently, and the median value (the percentage of cells with abnormal nuclei) was calculated and plotted.

siRNA sequences and transfection protocol

The following siRNA duplexes were used at a final concentration of 37.5 nM: control siRNA (Thermo Scientific siGENOME Non-Targeting siRNA #1 D-001210-01 and #4 D-001210-04, RISC free siRNA D-001220-01) and Thermo Scientific siGENOME smartpool siRNAs targeting Mad2 (M-003271-01), ESCO1 (M-023413-01), ESCO2 (M-025788-01), MFAP1 (M-020071-01), SART1 (M-017283-01), NHP2L1 (M-019900-01), CDC5L (M-011237-00), SGOL1 (M-015475-01) and SCC1 (M-006832-01). siGENOME individual siRNAs were used against MFAP1 (D-020071-03) (Figs 1B–E, 2, 4–8, and Supplementary Figs S4, S6 and S8), SART1 (D-017283-02) (Figs 4–8 and Supplementary Figs S4, S6 and S8), NHP2L1 (D-019900-02) (Figs 4–8 and Supplementary Figs S4, S6 and S8), CDC5L (D-011237-04) (Figs 4–8 and Supplementary Fig S8), sororin (D-015256-06) (Figs 4–8, and Supplementary Figs S4, S6 and S8), SGOL1 (D-015475-17) (Figs 4–8), SCC1 (D-006832-03) (Figs 4–8) and WAPL (D-015475-17). siRNA against SCC4 (corresponding to the sequence ACACAUUGCUGGGCCUGUAUU) was obtained from Sigma-Aldrich. The siRNA transfections were performed using a reverse transfection protocol with Lipofectamine RNAiMAX (Invitrogen) as per the manufacturer's instructions. Briefly, siRNAs at a concentration of 37.5 nM were diluted with OptiMEM (GIBCO) and mixed with appropriate volume of RNAiMAX as per surface area of the wells. After incubating for 15 min at room temperature, the mixture was added to appropriate number of cells in DMEM medium. Cells were then incubated for the indicated durations and processed for experiments.

Generation of stable cell lines using plasmid transfection

To create tagged versions of the genes used in the study (MFAP1, NHP2L1, SART1) for expression in human cells, AcGFP (Aequorea coerulescens GFP) was amplified from pAcGFP-N1 (Clontech) and inserted into pIRESpuro3 (Clontech). During amplification, a Kozak sequence (CGCCACC) and a FLAG epitope (DYKDDDDK) were added to AcGFP before the start codon and after the last amino acid, respectively, creating pIRESpuro3-AcFL (Su *et al*, 2011; Lekomtsev *et al*, 2012). The coding sequences of MFAP1, NHP2L1 and SART1 were amplified from cDNA (Source Biosciences) and introduced into pIRESpuro3-AcFL using the restriction enzymes AgeI and EcoRI. To create siRNA-resistant variant of the genes, the following sequences were mutated using the Quikchange II site directed mutagenesis kit (Stratagene) (underlined are the silent nucleotide substitutions). For MFAP1, the sequence aagtgaaggtaaagcgtta was mutated to aggttaaagtgaaacgcta; for NHP2L1, the sequence ttgaaaggctcttagtcta was mutated to ttgagagactgttggtgta; and for SART1, the sequence gcaagagcatgaacgcgaa was mutated to gcaaaagtatgaatgccaa. The plasmids were transfected into HeLa Kyoto cells using FuGENE 6 transfection reagent (Roche). Clonal cell lines were isolated after 2 weeks of antibiotic selection and characterized by immunofluorescence microscopy and immunoblotting. HeLa Kyoto cells were transfected with a plasmid encoding nuclear-targeted RNase H1-EGFP [a generous gift from Robert Crouch (Cerritelli & Crouch, 2009)] following which GFP-positive cells were enriched by using fluorescence-activated cell sorting (FACS). Cells expressing H2B-mCherry were kindly provided by Su *et al* (2011) and were grown in DMEM media supplemented with 500 μg/ml G418 (Invitrogen). A cell line stably expressing H2B-mCherry and α-tubulin-GFP was kindly provided by Laurent Sansregret. Cells stably expressing SMC1-EGFP were used for photobleaching experiments and were a kind gift from Schmitz *et al* (2007).

Preparation of stable cells lines using lentiviral infection

To create tagged alleles of sororin for expression in human cells, the coding sequence of sororin was introduced into pIRESpuro3-AcFL using the restriction enzymes AgeI and EcoRI. To create an siRNA-resistant variant of sororin, the sequence cgcaggagccctaggattt was mutated to agaagatccccagaatct. After this, the entire AcFL-Sororin sequence was excised from pIRESpuro3 using the restriction enzymes ClaI and EcoRI and cloned into pLVX-puro (Clontech). HEK 293FT cells were pre-seeded and grown to about 50% confluency before being transfected with pLVX-puro-Sororin (WT or siRNA resistant) and a second-generation packaging system [psPAX2 and pMD2.G (Addgene)] using Lipofectamine 2000 (Invitrogen). Viral particles were collected 48 h after transfection by harvesting the supernatant and filtering it through a 0.45-μm PVDF filter unit (Millex HV). HeLa Kyoto cells were infected with different titres of viral particles in presence of 8 μg/ml polybrene (Sigma). The cells were grown for 48–60 h in the presence of viral particles before the medium was supplemented with 0.35–0.4 μg/ml puromycin (Sigma) for transgene selection. After passaging the cells for 3 generations, clonal cell lines were generated after 2 weeks of antibiotic

selection. The cell lines were characterized by immunofluorescence microscopy and immunoblotting.

Other cell lines

Cells expressing H2B-mCherry were kindly provided by Su *et al* (2011) and were grown in DMEM media supplemented with 500 μg/ml G418 (Invitrogen). A cell line stably expressing H2B-mCherry and α-tubulin-GFP was kindly provided by Laurent Sansregret. Cells stably expressing SMC1-EGFP were used for photobleaching experiments and were a kind gift from Schmitz *et al* (2007).

Cell synchronization and drug treatments

To synchronize cells, 2.5 mM thymidine (Sigma) was added to cells either at the time of transfection or 24 h later. At the time of release, cells were rinsed twice with DMEM and fresh medium was added. The cells were allowed to proceed through the cell cycle either for 3 h to enrich for cells in S phase (Fig 4C) or for 5 h to enrich cells in G2 phase (Figs 4A, 5, 6A–C, and 7A left panel). To synchronize cells for performing chromosome spreads, asynchronous HeLa Kyoto cells that were grown for 24, 30, 36 or 52 h after siRNA transfection were treated with 330 nM nocodazole (Sigma) for 4 h. To study mRNA half-life (Supplementary Fig S7A), asynchronous HeLa Kyoto cells were treated with 5 μg/ml actinomycin D (Sigma) and cells were harvested at the indicated time points after drug treatment for RNA analysis. To study protein half-life (Fig 6C and Supplementary Fig S7B), HeLa Kyoto cells were synchronized with 2.5 mM thymidine for 24 h following which they were released for 8 h and then treated with 30 ng/ml nocodazole for 5 h after which the cells were harvested by mitotic shake-off and allowed to re-enter the cell cycle. Two hours after release from nocodazole, cells were treated with either DMSO or 100 μg/ml cycloheximide (Sigma) and harvested at the indicated time points for protein analysis. To score for the ability of the cells to form a metaphase plate (Fig 1E), HeLa Kyoto cells were synchronized in metaphase by treatment for 3 h with the proteasome inhibitor MG132 at a final concentration of 10 μM.

Real-time PCR for measurement of RNA levels

The following primers were used for the real-time quantitative PCR (RT-qPCR) experiments (Fig 6B and Supplementary Fig S7A): sororin Exon1-Intron1 (Fwd: ACAGGTTCTAGAGACAGCGAG, Rev: AGTTATGTCTGGGAGGCGAA), sororin Exon2-Intron2 (Fwd: AGAGGGATGAACGTGAGCTC, Rev: AGGGCCCCATCTCCTACTAA), sororin Exon5 (Fwd: AAGTCAGGCGTTCCTACAGC, Rev: TCGAAGC CAAAGCAGGAC), SMC3 Exon1-Intron1 (Fwd: AGCAGTTTGCATT TTTACTTTGTTTA, Rev: TGCCAGTTCTTTCTGCTTTTC), SMC3 Exon1 (Fwd: AAGAGTGTATGAAGAAAATTCGAGAAC, Rev: GTTT GAGGCTCAGTGTCTGGT), SMC1A Exon9-Intron9 (Fwd: AGCATC AAGCGCCTTTACCC, Rev: GGATTGGCAACCCTGTCCTTA), SMC1A Exon9 (Fwd: GACAGAGGAGGTGGAGATGG, Rev: CAGGGTAAAGG CGCTTGATG), SCC1 Intron1-Exon2 (Fwd: AAAGAAGACTAT-GAATGGCACGA, Rev: AGTCTGCAAGAAGGTATTTGGC), SCC1 Exon1 (Fwd: TCTACGCACATTTTGTTCTCAGT, Rev: TACACTC-GAACACATGGGCT), SA2 Exon4-Intron4 (Fwd: AGCATGACCGAG-ATATAGCACT, Rev: GTGACTATTTGAGAGCTGCTGA), SA2 Exon6 (Fwd: AGATTATCCACTTACCATGGCTG, Rev: CCAGGGTGCTTGTA TGTCGA) and GAPDH (Fwd: CCTCCCGCTTCGCTCCT, Rev: CTGGCGACGCAAAAGAAGA). G2 synchronized HeLa Kyoto cells transfected with the indicated siRNAs (Fig 6B) or asynchronous HeLa Kyoto cells treated with DMSO or 5 μg/ml actinomycin D (Supplementary Fig S7A) were harvested and lysed in RLT plus buffer (Qiagen RNeasy Plus kit) + β-mercaptoethanol (Sigma). RNA was extracted from the cells using the RNeasy plus MiniKit (Qiagen) according to the manufacturer's instructions. After measuring the RNA concentration in a NanoDrop spectrophotometer, 1.5 μg of total RNA was reverse transcribed with random hexamer primers using the TaqMan reverse transcription kit (Applied Biosystems). Pre-mRNA and mature mRNA levels were assessed by real-time quantitative PCR (RT-qPCR) performed using the indicated primer pairs using iQ-SYBR Green Supermix and CFX96 Real-Time System (Bio-Rad) using the manufacturer's instructions. The relative amount of RNA was calculated using the $\Delta\Delta C_t$ method as described earlier (Winer *et al*, 1999). GAPDH mRNA was chosen for normalization of the mRNA measurements (Fig 6B and Supplementary Fig S7A).

Immunofluorescence microscopy (IF)

Cells grown on coverslips with a diameter of 18 mm and thickness 1 (Assistent) were fixed overnight with methanol at −20°C or for 10 min at 37°C in 4% formaldehyde in PBS (Thermo Scientific, 16% PFA stock diluted with PBS). After fixation, samples were washed three times in 0.01% Triton X-100 in PBS for 5 min each and then permeabilized with 0.2% Triton X-100 in PBS for 10 min. Following three washes in 0.01% Triton X-100 in PBS, the coverslips were incubated with blocking solution (3% BSA in PBS containing 0.01% Triton X-100) for 1 h. Samples were incubated with the primary antibody in the blocking solution at 4°C overnight. Samples were then washes with three times with 0.01% Triton X-100 in PBS being incubated with secondary antibody diluted in blocking solution for 1 h along with 1 μg/ml DAPI. Following three more washes with 0.01% Triton X-100 in PBS, the coverslips were mounted onto microscopic slides with ProLong Gold (Molecular Probes) and left to dry overnight. Images were acquired on Zeiss Axio Imager M1 or M2 microscopes using a Plan Neofluor 40× /1.3 oil objective lens or 63× /1.4 Apochromat oil objective lens (Zeiss) equipped with an ORCA-ER camera (Hamamatsu) and controlled by Volocity 6.1. software (Improvision). Images were deconvolved using Volocity's iterative restoration function. The images were processed using ImageJ and Adobe Photoshop software.

Antibodies and dyes

The following primary antibodies were used in this study for immunoblotting (IB) and immunofluorescence (IF) experiments: mouse monoclonal anti-AcGFP (JL8, Clontech, IF & IB 1:2,000), rabbit anti-AcGFP (Clontech, IF & IB 1:2,000), mouse monoclonal anti-α-tubulin (B512, Sigma, IF & IB 1:10,000), rabbit monoclonal anti-β-tubulin HRP Conjugate (9F3, Cell Signaling, IB 1:2,000), mouse monoclonal anti-SMC1 (6892, Cell Signalling, IB 1:1,000), rabbit polyclonal anti-SMC3 (ab9263, Abcam, IB 1:2,000), rabbit monoclonal anti-SA2 (5882, Cell Signalling, IB 1:1,000), rabbit polyclonal anti-MFAP1 (SAB2104903, Sigma, IB 1:2,000), rabbit polyclonal anti-NHP2L1 (95958, Abcam IB 1:5,000) and rabbit polyclonal anti-SART1 (SC376460, Santa Cruz, IB 1:1,000). Jan-Michael Peters (IMP,

Vienna) kindly provided the following antibodies: rabbit polyclonal anti-SGOL1 (#975, IB 1:500), rabbit polyclonal anti-sororin (#953, IB 1:2,000), rabbit polyclonal anti-SCC4 (#974, IB 1:1,000) and rabbit polyclonal anti-SCC1 (#890, IB 1:1,000). Katsuhiko Shirahige (University of Tokyo) kindly provided a monoclonal mouse antibody recognizing SMC3 acetylated at Lys105 and Lys106 (IB 1:1,000) (Nishiyama *et al*, 2010). Secondary antibodies conjugated to either Alexa Fluor 488 or 594 (Molecular Probes) at a final dilution of 1:1,000 were used for IF detection. DNA was stained with 1 μg/ml DAPI (Molecular Probes). HRP-conjugated secondary antibodies at a concentration of 1:5,000 were used to detect proteins on immunoblots using chemiluminescence (GE Healthcare). For fluorescent detection of Western blotting, anti-rabbit IgG conjugate (Dylight R 680) and anti-mouse IgG conjugate (Dylight R 800) (Cell Signalling) at a final concentration of 1:15,000 were used for detection with Odyssey Imaging System (LI-COR Biosciences).

Time-lapse microscopy

To quantify mitotic duration and cell division status (Fig 1B and C), cells were seeded in 12-well plates (Nunc). An hour prior to imaging, the medium was changed to CO_2-independent medium without phenol red (Invitrogen) supplemented with 10% FCS, 0.2 mM L-glutamine, PenStrep, and 1 mM Na-pyruvate (all Invitrogen). Phase contrast images of cells were acquired every 5 min at 37°C using a Zeiss Axio Observer Z1 microscope controlled by SimplePCI software (Hamamatsu) equipped with an Orca 03GO1 camera (Hamamatsu) and a Plan-Apochromat 10×/0.45 objective.

To quantify mitotic duration for Supplementary Fig S8A, cells were reverse transfected with the indicated siRNAs in 24-well Imagelock plates (Essen BioScience). 12 h after seeding, the plate was imaged using an Incucyte live cell imaging system (Essen BioScience). Images were processed using ImageJ software and analysed using the mitotic duration plugin. For high resolution imaging (Fig 1D), HeLa Kyoto cells stably expressing H2B-mCherry and α-tubulin-GFP were seeded in Labtek chambers (Nunc, Thermo Scientific) and imaged at intervals of 5 min using a Zeiss Axio Observer Z1 microscope controlled by SimplePCI software (Hamamatsu) with a 40× /1.3 DIC H oil objective.

Chromosome spreads

Chromosome spreads of HeLa Kyoto and HCT116 cells were performed as follows. Cells transfected with the indicated siRNAs at a final concentration of 37.5 nM were grown at 37°C for 24, 30, 36 or 52 h as indicated. To enrich for mitotic cells, the medium was supplemented with 330 nM nocodazole for 4 h. Cells were harvested by mitotic shake-off and centrifugation. Subsequently, cells were incubated in a hypotonic solution (DMEM: filtered deionized water at 1:2) for 6 min at room temperature (RT). Cells were subsequently fixed with freshly made Carnoy's buffer (1:3 Glacial acetic acid: methanol) for 15 min at RT and pelleted. This fixation step was repeated three times. The suspension of cells in Carnoy's buffer was dropped onto a clean slide from a distance of 2 feet and left to dry overnight at RT. The slides were washed in PBS solution containing 1 μg/ml DAPI and mounted using Prolong Gold mounting solution. Chromosome spreads from individual cells were classified and scored with regards to the status of sister chromatid cohesion based on the indicated morphological criteria (normal X-shaped/parallel/split) and represented in graphs. Within a single karyotype, the majority of chromatids and chromosomes typically conformed to one of the categories used and the spread was therefore classified accordingly. For sister chromatid cohesion percentage data associated with micrographs, the categories of parallel and fully split chromatids were combined.

Fluorescence *in situ* hybridization (FISH) in mitotic cells

To analyse the status of sister chromatid cohesion in intact mitotic cells, we performed FISH experiments (Fig 2B). Cells were reverse transfected with indicated siRNAs onto 18-mm coverslips and grown for 48 h. Subsequently, the cells on the coverslips were fixed with Carnoy's buffer for 15 min at RT. FISH probes for the centromeres of chromosomes 6 (LPE 06G) and chromosome 8 (LPE 08R) (Cytocell aquarius) were used to probe the status of sister chromatid cohesion. The FISH probes were diluted in hybridization buffer (Cytocell aquarius) 1:10 and subsequently added to the fixed coverslips. Denaturation was performed for 3 min at 75°C, and the slide was left to hybridize overnight at 37°C in a humidified and lightproof chamber. Following this, the coverslip was washed in 0.25× SSC for 3 min at 73°C and subsequently in 2× SSC with 0.05% Tween 20 for 30 s at RT. The coverslips were then incubated in PBS containing 1 μg/ml DAPI to counterstain DNA. Finally, the coverslips were mounted using Prolong Gold mounting solution. Images were then acquired on a Zeiss Axio Imager M2 microscope using a Plan Neofluor 40×/1.3 oil objective lens equipped with an ORCA-ER camera (Hamamatsu) and controlled by Volocity 6.1 software (Improvision). Distance measurements were performed in Volocity by locating the centres of each of the pair of centroids manually and measuring the distance along a straight line between the two centroids. If the distance between two closest signals for a chromosome was larger than 2 μm, they were considered to be split.

FISH in interphase cells

Interphase FISH experiments (Fig 4A) were performed as previously described (Schmitz *et al*, 2007). Briefly, cells were transfected with the indicated siRNA duplexes on coverslips with a diameter of 18 mm and thickness 1 (Assistent). 2.5 mM thymidine was added either at the time of transfection or 24 h later. Following 24 h of thymidine arrest, cells were released from the thymidine arrest by rinsing twice in DMEM and then allowed to proceed through the cell cycle. 5 h after release, they were fixed with Carnoy's buffer (15 min at RT) and left to dry overnight. BAC clone RP11-113F1 corresponding to the human *tff1* locus was kindly provided by Erwan Watrin (University of Rennes). The BAC was used to generate FISH probes labelled with PrimeIt II Random primer labelling kit (Stratagene) and Cy3-dCTP (Amersham Biosciences) as described earlier (Schmitz *et al*, 2007). Just before use, the probes were diluted in hybridization buffer (Cytocell Aquarius) 1:10. The probe was added to the fixed coverslips. The coverslip, along with the probes were denatured for 3 min at 75°C. Subsequently, they were incubated in a humidified chamber at 37°C overnight. After the incubation, the coverslips were washed briefly in 0.4× SSC made from a stock of 20× SSC (3M NaCl + 300 mM $Na_3C_6H_5O_7$) at 72°C for 3 min and then in 2× SSC with 0.05% Tween 20 at RT for 30 s.

Following this, DNA was counterstained with 1 μg/ml DAPI and the coverslips were mounted with ProLong Gold (Molecular Probes). Images were acquired on a Zeiss Axio Imager M1 microscope using a Plan Neofluor 40×/1.3 oil objective lens equipped with an ORCA-ER camera (Hamamatsu) and controlled by Volocity 6.1. software (Improvision). Images were deconvolved using Volocity's iterative restoration function. Distance measurements were performed in Volocity by locating the centres of each of the pair of centroids manually and measuring the distance along a straight line between the two centroids. In control and SGOL1 depleted cells, since the distances were often difficult to resolve because of the proximity of the dots. As a consequence, only cells where at least 2 out of the 3 centroid pairs were resolvable were considered for the analysis. In sororin, MFAP1, NHP2L1 and SART1 depleted cells, the vast majority of paired signals were clearly resolved and could be measured.

Photobleaching experiments

Photobleaching experiments (Fig 5) were performed as described previously (Gerlich *et al*, 2006; Schmitz *et al*, 2007). Cells stably expressing SMC1-EGFP, obtained from Schmitz *et al* (2007), were reverse transfected with the indicated siRNA duplexes at a final concentration of 37.5 nM in Labtek 2 chambered borosilicate coverglass chambers (Nunc, Thermo Scientific). 2.5 mM thymidine was added either at the time of seeding or 24 h post-seeding. Cells were released from thymidine arrest after 24 h (by rinsing twice in DMEM) and allowed to proceed through the cell cycle for 5 h. An hour before imaging, the medium was changed to CO_2-independent medium without phenol red (Invitrogen) supplemented with 10% FCS, 0.2 mM L-glutamine, PenStrep and 1 mM Na-pyruvate (all Invitrogen). 1 μg/ml cycloheximide (Sigma) was added to avoid new synthesis of SMC1-EGFP. The imaging and bleaching was performed at 37°C using a Olympus FV1000D (InvertedMicroscopeIX81) laser confocal scanning microscope equipped with a PlanApoN ×60/1.40 NA Oil Sc objective lens and controlled by FV10-ASW software (Olympus). One half of the nuclear region was bleached leaving the other half intact. Repeated bleaching was performed every 10 s for five iterations in order to remove the soluble pool of SMC1-EGFP. This resulted in a reduction in the fluorescence intensity of the unbleached nuclear area as well. The first post-bleach frame used for the downstream analysis was acquired 2 min after photobleaching to allow for complete equilibration of bleached soluble SMC1-EGFP across the nucleus. ImageJ software was used for the intensity measurements. EGFP intensities were measured by drawing a rectangular area of the same dimensions in the bleached and unbleached area followed by subtraction of the mean background signal outside of the cell. The difference between the background corrected mean fluorescence intensity of the unbleached and bleached area normalized to the difference in the first post-bleach frame was calculated and plotted over time for the different siRNA treatments.

Supplementary information for this article is available online: http://emboj.embopress.org

Acknowledgements

We are grateful to Robert Crouch, Petra van der Lelij, Jan-Michael Peters, Laurent Sansregret, Katsuhiko Shirahighe and Erwan Watrin for reagents, discussions and advice; to Marco Saponaro for help with RT-qPCR experiments; and to Antonio Tedeschi for critical reading of the manuscript. Work in the Petronczki laboratory is supported by Cancer Research UK, the EMBO Young Investigator Programme and a Breast Cancer Campaign PhD grant to SS and MP (2009NovPhD14).

Author contributions

MP and SS designed the study. SS performed and analysed most of the experiments with contributions from MDVN and SL. The siRNA screen was carried out in collaboration with MH. MP and SS wrote the manuscript.

Conflict of interest

The authors declare that they have no conflict of interest.

References

Aguilera A, Garcia-Muse T (2012) R loops: from transcription byproducts to threats to genome stability. *Mol Cell* 46: 115 – 124

Ajuh P, Kuster B, Panov K, Zomerdijk JC, Mann M, Lamond AI (2000) Functional analysis of the human CDC5L complex and identification of its components by mass spectrometry. *EMBO J* 19: 6569 – 6581

Andersen DS, Tapon N (2008) Drosophila MFAP1 is required for pre-mRNA processing and G2/M progression. *J Biol Chem* 283: 31256 – 31267

Braunschweig U, Gueroussov S, Plocik AM, Graveley BR, Blencowe BJ (2013) Dynamic integration of splicing within gene regulatory pathways. *Cell* 152: 1252 – 1269

Buheitel J, Stemmann O (2013) Prophase pathway-dependent removal of cohesin from human chromosomes requires opening of the Smc3-Scc1 gate. *EMBO J* 32: 666 – 676

Burns CG, Ohi R, Mehta S, O'Toole ET, Winey M, Clark TA, Sugnet CW, Ares M Jr, Gould KL (2002) Removal of a single alpha-tubulin gene intron suppresses cell cycle arrest phenotypes of splicing factor mutations in *Saccharomyces cerevisiae*. *Mol Cell Biol* 22: 801 – 815

Cerritelli SM, Crouch RJ (2009) Ribonuclease H: the enzymes in eukaryotes. *FEBS J* 276: 1494 – 1505

Chan KL, Roig MB, Hu B, Beckouet F, Metson J, Nasmyth K (2012) Cohesin's DNA exit gate is distinct from its entrance gate and is regulated by acetylation. *Cell* 150: 961 – 974

Ciosk R, Shirayama M, Shevchenko A, Tanaka T, Toth A, Shevchenko A, Nasmyth K (2000) Cohesin's binding to chromosomes depends on a separate complex consisting of Scc2 and Scc4 proteins. *Mol Cell* 5: 243 – 254

Conery AR, Harlow E (2010) High-throughput screens in diploid cells identify factors that contribute to the acquisition of chromosomal instability. *Proc Natl Acad Sci USA* 107: 15455 – 15460

Daum JR, Potapova TA, Sivakumar S, Daniel JJ, Flynn JN, Rankin S, Gorbsky GJ (2011) Cohesion fatigue induces chromatid separation in cells delayed at metaphase. *Curr Biol* 21: 1018 – 1024

Eichinger CS, Kurze A, Oliveira RA, Nasmyth K (2013) Disengaging the Smc3/kleisin interface releases cohesin from *Drosophila* chromosomes during interphase and mitosis. *EMBO J* 32: 656 – 665

Folco EG, Coil KE, Reed R (2011) The anti-tumor drug E7107 reveals an essential role for SF3b in remodeling U2 snRNP to expose the branch point-binding region. *Genes Dev* 25: 440 – 444

Gandhi R, Gillespie PJ, Hirano T (2006) Human Wapl is a cohesin-binding protein that promotes sister-chromatid resolution in mitotic prophase. *Curr Biol* 16: 2406 – 2417

Gentien D, Kosmider O, Nguyen-Khac F, Albaud B, Rapinat A, Dumont AG, Damm F, Popova T, Marais R, Fontenay M, Roman-Roman S, Bernard OA,

Stern MH (2014) A common alternative splicing signature is associated with SF3B1 mutations in malignancies from different cell lineages. *Leukemia* 28: 1355 – 1357

Gerlich D, Koch B, Dupeux F, Peters JM, Ellenberg J (2006) Live-cell imaging reveals a stable cohesin-chromatin interaction after but not before DNA replication. *Curr Biol* 16: 1571 – 1578

Gimenez-Abian JF, Sumara I, Hirota T, Hauf S, Gerlich D, de la Torre C, Ellenberg J, Peters JM (2004) Regulation of sister chromatid cohesion between chromosome arms. *Curr Biol* 14: 1187 – 1193

Grote M, Wolf E, Will CL, Lemm I, Agafonov DE, Schomburg A, Fischle W, Urlaub H, Luhrmann R (2010) Molecular architecture of the human Prp19/CDC5L complex. *Mol Cell Biol* 30: 2105 – 2119

Guacci V, Hogan E, Koshland D (1994) Chromosome condensation and sister chromatid pairing in budding yeast. *J Cell Biol* 125: 517 – 530

Gullerova M, Proudfoot NJ (2008) Cohesin complex promotes transcriptional termination between convergent genes in *S. pombe*. *Cell* 132: 983 – 995

Haarhuis JH, Elbatsh AM, van den Broek B, Camps D, Erkan H, Jalink K, Medema RH, Rowland BD (2013) WAPL-mediated removal of cohesin protects against segregation errors and aneuploidy. *Curr Biol* 23: 2071 – 2077

Hadjur S, Williams LM, Ryan NK, Cobb BS, Sexton T, Fraser P, Fisher AG, Merkenschlager M (2009) Cohesins form chromosomal cis-interactions at the developmentally regulated IFNG locus. *Nature* 460: 410 – 413

Haering CH, Farcas AM, Arumugam P, Metson J, Nasmyth K (2008) The cohesin ring concatenates sister DNA molecules. *Nature* 454: 297 – 301

Hauf S, Waizenegger IC, Peters JM (2001) Cohesin cleavage by separase required for anaphase and cytokinesis in human cells. *Science* 293: 1320 – 1323

Hauf S, Roitinger E, Koch B, Dittrich CM, Mechtler K, Peters JM (2005) Dissociation of cohesin from chromosome arms and loss of arm cohesion during early mitosis depends on phosphorylation of SA2. *PLoS Biol* 3: e69

Hofmann JC, Husedzinovic A, Gruss OJ (2010) The function of spliceosome components in open mitosis. *Nucleus* 1: 447 – 459

Hofmann JC, Tegha-Dunghu J, Drager S, Will CL, Luhrmann R, Gruss OJ (2013) The Prp19 complex directly functions in mitotic spindle assembly. *PLoS ONE* 8: e74851

Horsfield JA, Anagnostou SH, Hu JK, Cho KH, Geisler R, Lieschke G, Crosier KE, Crosier PS (2007) Cohesin-dependent regulation of Runx genes. *Development* 134: 2639 – 2649

Hou F, Zou H (2005) Two human orthologues of Eco1/Ctf7 acetyltransferases are both required for proper sister-chromatid cohesion. *Mol Biol Cell* 16: 3908 – 3918

Huen MS, Sy SM, Leung KM, Ching YP, Tipoe GL, Man C, Dong S, Chen J (2010) SON is a spliceosome-associated factor required for mitotic progression. *Cell Cycle* 9: 2679 – 2685

Jurica MS, Moore MJ (2003) Pre-mRNA splicing: awash in a sea of proteins. *Mol Cell* 12: 5 – 14

Kim ST, Xu B, Kastan MB (2002) Involvement of the cohesin protein, Smc1, in Atm-dependent and independent responses to DNA damage. *Genes Dev* 16: 560 – 570

Kitajima TS, Kawashima SA, Watanabe Y (2004) The conserved kinetochore protein shugoshin protects centromeric cohesion during meiosis. *Nature* 427: 510 – 517

Kittler R, Pelletier L, Heninger A-K, Slabicki M, Theis M, Miroslaw L, Poser I, Lawo S, Grabner H, Kozak K, Wagner J, Surendranath V, Richter C, Bowen W, Jackson AL, Habermann B, Hyman AA, Buchholz F (2007) Genome-scale RNAi profiling of cell division in human tissue culture cells. *Nat Cell Biol* 9: 1401 – 1412

Kueng S, Hegemann B, Peters BH, Lipp JJ, Schleiffer A, Mechtler K, Peters JM (2006) Wapl controls the dynamic association of cohesin with chromatin. *Cell* 127: 955 – 967

Lafont AL, Song J, Rankin S (2010) Sororin cooperates with the acetyltransferase Eco2 to ensure DNA replication-dependent sister chromatid cohesion. *Proc Natl Acad Sci USA* 107: 20364 – 20369

Landeira D, Bart JM, Van Tyne D, Navarro M (2009) Cohesin regulates VSG monoallelic expression in trypanosomes. *J Cell Biol* 186: 243 – 254

Lara-Gonzalez P, Westhorpe FG, Taylor SS (2012) The spindle assembly checkpoint. *Curr Biol* 22: R966 – R980

Lee KM, Tarn WY (2013) Coupling pre-mRNA processing to transcription on the RNA factory assembly line. *RNA Biol* 10: 380 – 390

Lekomtsev S, Su KC, Pye VE, Blight K, Sundaramoorthy S, Takaki T, Collinson LM, Cherepanov P, Divecha N, Petronczki M (2012) Centralspindlin links the mitotic spindle to the plasma membrane during cytokinesis. *Nature* 492: 276 – 279

van der Lelij P, Stocsits R, Ladurner R, Petzold G, Kreidl E, Koch B, Schmitz J, Neumann B, Ellenberg J, Peters JM (2014) SNW1 enables sister chromatid cohesion by mediating the splicing of sororin and APC2 pre-mRNAs. *EMBO J* 33: 2643 – 2658

Lengronne A, Katou Y, Mori S, Yokobayashi S, Kelly GP, Itoh T, Watanabe Y, Shirahige K, Uhlmann F (2004) Cohesin relocation from sites of chromosomal loading to places of convergent transcription. *Nature* 430: 573 – 578

Li X, Manley JL (2005) Inactivation of the SR protein splicing factor ASF/SF2 results in genomic instability. *Cell* 122: 365 – 378

Losada A, Hirano M, Hirano T (2002) Cohesin release is required for sister chromatid resolution, but not for condensin-mediated compaction, at the onset of mitosis. *Genes Dev* 16: 3004 – 3016

Makarova OV, Makarov EM, Luhrmann R (2001) The 65 and 110 kDa SR-related proteins of the U4/U6.U5 tri-snRNP are essential for the assembly of mature spliceosomes. *EMBO J* 20: 2553 – 2563

Makarova OV, Makarov EM, Urlaub H, Will CL, Gentzel M, Wilm M, Luhrmann R (2004) A subset of human 35S U5 proteins, including Prp19, function prior to catalytic step 1 of splicing. *EMBO J* 23: 2381 – 2391

Matsunaga S, Takata H, Morimoto A, Hayashihara K, Higashi T, Akatsuchi K, Mizusawa E, Yamakawa M, Ashida M, Matsunaga TM, Azuma T, Uchiyama S, Fukui K (2012) RBMX: a regulator for maintenance and centromeric protection of sister chromatid cohesion. *Cell Rep* 1: 299 – 308

McCracken S, Longman D, Marcon E, Moens P, Downey M, Nickerson JA, Jessberger R, Wilde A, Caceres JF, Emili A, Blencowe BJ (2005) Proteomic analysis of SRm160-containing complexes reveals a conserved association with cohesin. *J Biol Chem* 280: 42227 – 42236

McGuinness BE, Hirota T, Kudo NR, Peters JM, Nasmyth K (2005) Shugoshin prevents dissociation of cohesin from centromeres during mitosis in vertebrate cells. *PLoS Biol* 3: e86

Mukherji M, Bell R, Supekova L, Wang Y, Orth AP, Batalov S, Miraglia L, Huesken D, Lange J, Martin C, Sahasrabudhe S, Reinhardt M, Natt F, Hall J, Mickanin C, Labow M, Chanda SK, Cho CY, Schultz PG (2006) Genome-wide functional analysis of human cell-cycle regulators. *Proc Natl Acad Sci USA* 103: 14819 – 14824

Nasmyth K, Haering CH (2009) Cohesin: its roles and mechanisms. *Annu Rev Genet* 43: 525 – 558

Nativio R, Wendt KS, Ito Y, Huddleston JE, Uribe-Lewis S, Woodfine K, Krueger C, Reik W, Peters JM, Murrell A (2009) Cohesin is required for higher-order

chromatin conformation at the imprinted IGF2-H19 locus. *PLoS Genet* 5: e1000739

Neumann B, Walter T, Heriche JK, Bulkescher J, Erfle H, Conrad C, Rogers P, Poser I, Held M, Liebel U, Cetin C, Sieckmann F, Pau G, Kabbe R, Wunsche A, Satagopam V, Schmitz MH, Chapuis C, Gerlich DW, Schneider R *et al* (2010) Phenotypic profiling of the human genome by time-lapse microscopy reveals cell division genes. *Nature* 464: 721 – 727

Nishiyama T, Ladurner R, Schmitz J, Kreidl E, Schleiffer A, Bhaskara V, Bando M, Shirahige K, Hyman AA, Mechtler K, Peters JM (2010) Sororin mediates sister chromatid cohesion by antagonizing Wapl. *Cell* 143: 737 – 749

Nishiyama T, Sykora MM, Huis In 't Veld PJ, Mechtler K, Peters JM (2013) Aurora B and Cdk1 mediate Wapl activation and release of acetylated cohesin from chromosomes by phosphorylating Sororin. *Proc Natl Acad Sci USA* 110: 13404 – 13409

Oliveira RA, Hamilton RS, Pauli A, Davis I, Nasmyth K (2010) Cohesin cleavage and Cdk inhibition trigger formation of daughter nuclei. *Nat Cell Biol* 12: 185 – 192

Papaemmanuil E, Cazzola M, Boultwood J, Malcovati L, Vyas P, Bowen D, Pellagatti A, Wainscoat JS, Hellstrom-Lindberg E, Gambacorti-Passerini C, Godfrey AL, Rapado I, Cvejic A, Rance R, McGee C, Ellis P, Mudie LJ, Stephens PJ, McLaren S, Massie CE *et al* (2011) Somatic SF3B1 mutation in myelodysplasia with ring sideroblasts. *N Engl J Med* 365: 1384 – 1395

Parelho V, Hadjur S, Spivakov M, Leleu M, Sauer S, Gregson HC, Jarmuz A, Canzonetta C, Webster Z, Nesterova T, Cobb BS, Yokomori K, Dillon N, Aragon L, Fisher AG, Merkenschlager M (2008) Cohesins functionally associate with CTCF on mammalian chromosome arms. *Cell* 132: 422 – 433

Pauli A, van Bemmel JG, Oliveira RA, Itoh T, Shirahige K, van Steensel B, Nasmyth K (2010) A direct role for cohesin in gene regulation and ecdysone response in Drosophila salivary glands. *Curr Biol* 20: 1787 – 1798

Quesada V, Conde L, Villamor N, Ordonez GR, Jares P, Bassaganyas L, Ramsay AJ, Bea S, Pinyol M, Martinez-Trillos A, Lopez-Guerra M, Colomer D, Navarro A, Baumann T, Aymerich M, Rozman M, Delgado J, Gine E, Hernandez JM, Gonzalez-Diaz M *et al* (2012) Exome sequencing identifies recurrent mutations of the splicing factor SF3B1 gene in chronic lymphocytic leukemia. *Nat Genet* 44: 47 – 52

Rankin S, Ayad NG, Kirschner MW (2005) Sororin, a substrate of the anaphase-promoting complex, is required for sister chromatid cohesion in vertebrates. *Mol Cell* 18: 185 – 200

Rolef Ben-Shahar T, Heeger S, Lehane C, East P, Flynn H, Skehel M, Uhlmann F (2008) Eco1-dependent cohesin acetylation during establishment of sister chromatid cohesion. *Science* 321: 563 – 566

Rollins RA, Korom M, Aulner N, Martens A, Dorsett D (2004) Drosophila nipped-B protein supports sister chromatid cohesion and opposes the stromalin/Scc3 cohesion factor to facilitate long-range activation of the cut gene. *Mol Cell Biol* 24: 3100 – 3111

Rossi D, Bruscaggin A, Spina V, Rasi S, Khiabanian H, Messina M, Fangazio M, Vaisitti T, Monti S, Chiaretti S, Guarini A, Del Giudice I, Cerri M, Cresta S, Deambrogi C, Gargiulo E, Gattei V, Forconi F, Bertoni F, Deaglio S *et al* (2011) Mutations of the SF3B1 splicing factor in chronic lymphocytic leukemia: association with progression and fludarabine-refractoriness. *Blood* 118: 6904 – 6908

Rowland BD, Roig MB, Nishino T, Kurze A, Uluocak P, Mishra A, Beckouet F, Underwood P, Metson J, Imre R, Mechtler K, Katis VL, Nasmyth K (2009) Building sister chromatid cohesion: smc3 acetylation counteracts an antiestablishment activity. *Mol Cell* 33: 763 – 774

Rubio ED, Reiss DJ, Welcsh PL, Disteche CM, Filippova GN, Baliga NS, Aebersold R, Ranish JA, Krumm A (2008) CTCF physically links cohesin to chromatin. *Proc Natl Acad Sci USA* 105: 8309 – 8314

Salic A, Waters JC, Mitchison TJ (2004) Vertebrate shugoshin links sister centromere cohesion and kinetochore microtubule stability in mitosis. *Cell* 118: 567 – 578

Schmitz J, Watrin E, Lenart P, Mechtler K, Peters JM (2007) Sororin is required for stable binding of cohesin to chromatin and for sister chromatid cohesion in interphase. *Curr Biol* 17: 630 – 636

Skop AR, Liu H, Yates J III, Meyer BJ, Heald R (2004) Dissection of the mammalian midbody proteome reveals conserved cytokinesis mechanisms. *Science* 305: 61 – 66

Skourti-Stathaki K, Proudfoot NJ, Gromak N (2011) Human senataxin resolves RNA/DNA hybrids formed at transcriptional pause sites to promote Xrn2-dependent termination. *Mol Cell* 42: 794 – 805

Sofueva S, Yaffe E, Chan WC, Georgopoulou D, Vietri Rudan M, Mira-Bontenbal H, Pollard SM, Schroth GP, Tanay A, Hadjur S (2013) Cohesin-mediated interactions organize chromosomal domain architecture. *EMBO J* 32: 3119 – 3129

Stedman W, Kang H, Lin S, Kissil JL, Bartolomei MS, Lieberman PM (2008) Cohesins localize with CTCF at the KSHV latency control region and at cellular c-myc and H19/Igf2 insulators. *EMBO J* 27: 654 – 666

Stevens D, Gassmann R, Oegema K, Desai A (2011) Uncoordinated loss of chromatid cohesion is a common outcome of extended metaphase arrest. *PLoS ONE* 6: e22969

Strom L, Lindroos HB, Shirahige K, Sjogren C (2004) Postreplicative recruitment of cohesin to double-strand breaks is required for DNA repair. *Mol Cell* 16: 1003 – 1015

Su KC, Takaki T, Petronczki M (2011) Targeting of the RhoGEF Ect2 to the equatorial membrane controls cleavage furrow formation during cytokinesis. *Dev Cell* 21: 1104 – 1115

Sumara I, Vorlaufer E, Stukenberg PT, Kelm O, Redemann N, Nigg EA, Peters JM (2002) The dissociation of cohesin from chromosomes in prophase is regulated by Polo-like kinase. *Mol Cell* 9: 515 – 525

Sutani T, Kawaguchi T, Kanno R, Itoh T, Shirahige K (2009) Budding yeast Wpl1(Rad61)-Pds5 complex counteracts sister chromatid cohesion-establishing reaction. *Curr Biol* 19: 492 – 497

Tanaka T, Fuchs J, Loidl J, Nasmyth K (2000) Cohesin ensures bipolar attachment of microtubules to sister centromeres and resists their precocious separation. *Nat Cell Biol* 2: 492 – 499

Tanaka K, Hao Z, Kai M, Okayama H (2001) Establishment and maintenance of sister chromatid cohesion in fission yeast by a unique mechanism. *EMBO J* 20: 5779 – 5790

Tedeschi A, Wutz G, Huet S, Jaritz M, Wuensche A, Schirghuber E, Davidson IF, Tang W, Cisneros DA, Bhaskara V, Nishiyama T, Vaziri A, Wutz A, Ellenberg J, Peters JM (2013) Wapl is an essential regulator of chromatin structure and chromosome segregation. *Nature* 501: 564 – 568

Uhlmann F, Nasmyth K (1998) Cohesion between sister chromatids must be established during DNA replication. *Curr Biol* 8: 1095 – 1101

Uhlmann F, Wernic D, Poupart MA, Koonin EV, Nasmyth K (2000) Cleavage of cohesin by the CD clan protease separin triggers anaphase in yeast. *Cell* 103: 375 – 386

Unal E, Arbel-Eden A, Sattler U, Shroff R, Lichten M, Haber JE, Koshland D (2004) DNA damage response pathway uses histone modification to assemble a double-strand break-specific cohesin domain. *Mol Cell* 16: 991 – 1002

Unal E, Heidinger-Pauli JM, Kim W, Guacci V, Onn I, Gygi SP, Koshland DE (2008) A molecular determinant for the establishment of sister chromatid cohesion. *Science* 321: 566 – 569

Wahl MC, Will CL, Luhrmann R (2009) The spliceosome: design principles of a dynamic RNP machine. *Cell* 136: 701 – 718

Waizenegger IC, Hauf S, Meinke A, Peters JM (2000) Two distinct pathways remove mammalian cohesin from chromosome arms in prophase and from centromeres in anaphase. *Cell* 103: 399 – 410

Wang L, Lawrence MS, Wan Y, Stojanov P, Sougnez C, Stevenson K, Werner L, Sivachenko A, DeLuca DS, Zhang L, Zhang W, Vartanov AR, Fernandes SM, Goldstein NR, Folco EG, Cibulskis K, Tesar B, Sievers QL, Shefler E, Gabriel S *et al* (2011) SF3B1 and other novel cancer genes in chronic lymphocytic leukemia. *N Engl J Med* 365: 2497 – 2506

Watrin E, Schleiffer A, Tanaka K, Eisenhaber F, Nasmyth K, Peters JM (2006) Human Scc4 is required for cohesin binding to chromatin, sister-chromatid cohesion, and mitotic progression. *Curr Biol* 16: 863 – 874

Watrin E, Peters JM (2009) The cohesin complex is required for the DNA damage-induced G2/M checkpoint in mammalian cells. *EMBO J* 28: 2625 – 2635

Wendt KS, Yoshida K, Itoh T, Bando M, Koch B, Schirghuber E, Tsutsumi S, Nagae G, Ishihara K, Mishiro T, Yahata K, Imamoto F, Aburatani H, Nakao M, Imamoto N, Maeshima K, Shirahige K, Peters JM (2008) Cohesin mediates transcriptional insulation by CCCTC-binding factor. *Nature* 451: 796 – 801

Winer J, Jung CK, Shackel I, Williams PM (1999) Development and validation of real-time quantitative reverse transcriptase-polymerase chain reaction for monitoring gene expression in cardiac myocytes *in vitro*. *Anal Biochem* 270: 41 – 49

Yamazaki T, Fujiwara N, Yukinaga H, Ebisuya M, Shiki T, Kurihara T, Kioka N, Kambe T, Nagao M, Nishida E, Masuda S (2010) The closely related RNA helicases, UAP56 and URH49, preferentially form distinct mRNA export machineries and coordinately regulate mitotic progression. *Mol Biol Cell* 21: 2953 – 2965

Yazdi PT, Wang Y, Zhao S, Patel N, Lee EY, Qin J (2002) SMC1 is a downstream effector in the ATM/NBS1 branch of the human S-phase checkpoint. *Genes Dev* 16: 571 – 582

Yoshida K, Sanada M, Shiraishi Y, Nowak D, Nagata Y, Yamamoto R, Sato Y, Sato-Otsubo A, Kon A, Nagasaki M, Chalkidis G, Suzuki Y, Shiosaka M, Kawahata R, Yamaguchi T, Otsu M, Obara N, Sakata-Yanagimoto M, Ishiyama K, Mori H *et al* (2011) Frequent pathway mutations of splicing machinery in myelodysplasia. *Nature* 478: 64 – 69

Yuce O, Piekny A, Glotzer M (2005) An ECT2-centralspindlin complex regulates the localization and function of RhoA. *J Cell Biol* 170: 571 – 582

Zhang J, Shi X, Li Y, Kim BJ, Jia J, Huang Z, Yang T, Fu X, Jung SY, Wang Y, Zhang P, Kim ST, Pan X, Qin J (2008) Acetylation of Smc3 by Eco1 is required for S phase sister chromatid cohesion in both human and yeast. *Mol Cell* 31: 143 – 151

Zhou Z, Licklider LJ, Gygi SP, Reed R (2002) Comprehensive proteomic analysis of the human spliceosome. *Nature* 419: 182 – 185

Zuin J, Dixon JR, van der Reijden MI, Ye Z, Kolovos P, Brouwer RW, van de Corput MP, van de Werken HJ, Knoch TA, van Ijcken WF, Grosveld FG, Ren B, Wendt KS (2014) Cohesin and CTCF differentially affect chromatin architecture and gene expression in human cells. *Proc Natl Acad Sci USA* 111: 996 – 1001

